High light-induced phosphorylation of Lhcb6 (CP24) enhances non-photochemical quenching dependent on the PSI-PSII megacomplexes

Yang Chunhong

yangch@ibcas.ac.cn

Institute of Botany, Chinese Academy of Sciences

lishuan wu

Key Laboratory of Plant Resources/Beijing Botanical Garden, Institute of Botany, the Chinese Academy of Sciences

Yajun Lin

CAS Center for Excellence in Molecular Plant Sciences / Institute of Plant Physiology and Ecology

Xinguang Zhu

CAS center for excellence in molecular plant sciences https://orcid.org/0000-0002-4435-130X

Yuanming Zhang

State Key Laboratory of Ecological Safety and Sustainable Development in Arid Lands, Xinjiang Institute of Ecology and Geography, Chinese Academy of Sciences

Article

Keywords: CP24, phosphorylation, non-photochemical quenching, mc1, spillover, photoprotection

Posted Date: October 29th, 2025

DOI: https://doi.org/10.21203/rs.3.rs-7613824/v1

Additional Declarations: There is **NO** Competing Interest.

High light-induced phosphorylation of Lhcb6 (CP24) enhances non-photochemical quenching dependent on the PSI-PSII megacomplexes

Abstract

Plants have evolved diverse photoprotective mechanisms to cope with fluctuating light environments, among which non-photochemical quenching (NPQ) plays a central role in dissipating excess excitation energy and preventing photosystem II (PSII) damage. While the molecular basis of NPQ is well established in model species such as *Arabidopsis thaliana*, its regulation in non-model plants remains less understood, offering untapped potential for discovering novel photoprotective strategies. Here, we report a previously unrecognized mechanism in angiosperms *Berteroa incana*: high light (HL)-induced phosphorylation of the minor antenna protein CP24 (Lhcb6), specifically at Thr178, serves as a critical regulator of NPQ, a close relative of *Arabidopsis thaliana* with exceptional phototolerance. Unlike LHCII phosphorylation mediated by STN7 kinases, CP24 phosphorylation is governed by a distinct kinase system and is selectively dephosphorylated by the phosphatase rPBCP. Using biochemical and functional analyses, we demonstrate that phosphorylated CP24 (P-CP24) predominantly resides within the PSII-PSI megacomplex (mc1), where it facilitates efficient energy transfer from CP47 to PSI. This mechanism drives a previously unreported Zeaxanthin- and Lutein-independent fluorescence quenching pathway under HL conditions in terrestrial plants. Our results suggest that P-CP24 enhances PSII photoprotection by dynamically redirecting excess excitation energy away from PSII reaction centers, thereby reducing reactive oxygen species (ROS) production, maintaining PSII activity, and optimizing energy utilization under stress.

Keywords: CP24, phosphorylation, non-photochemical quenching, mc1, spillover, photoprotection

Introduction

Oxygenic photosynthesis underpins global carbon fixation, sustaining nearly all life on earth by converting solar energy into chemical energy. However, excessive light exposure poses a major threat to photosynthetic machinery, particularly the reaction center of photosystem II (PSII), where the D1 protein is highly susceptible to photodamage[1,2]. Irreversible PSII reaction center damage triggers a progressive decline in maximum quantum yield of PSII (*Fv/Fm*), a hallmark of photoinhibition. To counteract photodamage, oxygenic phototrophs have evolved a range of photoprotective mechanisms[3-6]. Among these, non-photochemical quenching (NPQ) plays a central role by dissipating excess excitation energy as heat. Recent studies have revealed that NPQ can enhance photosynthetic efficiency, increase biomass accumulation, and improve the economic yields of crops, highlighting its potential as a target for crop improvement strategies[7-9].

NPQ comprises three major components: qE (energy-dependent quenching), qT (state transition quenching), and qI (irreversible/slowly reversible quenching) (Horton & Hague, 1988; Ferroni et al., 2014). The qT component is primarily mediated by phosphorylated light-harvesting complex II (P-LHCII). Under low light or PSII- preferred conditions, plastoquinone (PQ) pool reduction activates STN7 kinase, inducing maximal phosphorylation of Lhcb1/Lhcb2[10]. P-LHCII then migrates and binds to PSI via P- Lhcb2, forming the state 1 complex[11,12]. Conversely, under HL or PSI-preferred conditions trigger PQ pool oxidation, which inactivates STN7 through reduced thioredoxin[13]. The phosphatase TAP38/PPH1 subsequently dephosphorylates P-LHCII, facilitating its dissociation from PSI and return to PSII (state 2)[14,15].

In contrast to qT, qE dominates under high-light stress and is mainly regulated by conformational changes in the PSII antenna system triggered by lumen acidification[16,17]. This process is tightly linked to

the activity of the PsbS protein and the xanthophyll cycle, especially zeaxanthin accumulation[16–20]. HL also induces phosphorylation of PSII core proteins, including CP43, D2, D1. The STN8 kinase[13], phosphorylates these proteins to maintain structural integrity and facilitate their migration from grana to stroma by increasing thylakoid fluidity[21,22]. On the stromal side, the phosphatase PBCP reverses this modification, promoting D1 proteolysis and ribosome recruitment for PSII repair[23,24]. This phosphorylation/dephosphorylation cycle supports PSII repair and is closely associated with qI[25]. While both HL-induced PSII core phosphorylation and qE are elevated, they appear functionally uncoupled[26].

Notably, phosphorylated thylakoid membrane proteins have increasingly been recognized as important regulators of NPQ across diverse plant lineages. While much of our mechanistic understanding of NPQ comes from studies in the model species *Arabidopsis thaliana* (*A. thaliana*), recent evidence suggests that the roles and regulation of phosphorylated antenna proteins can vary significantly in other species. For instance, high-light induced phosphorylation of minor antenna proteins, such as CP29 in monocots like rice *Oryza sativa* (*O. sativa*)[26], CP24 in lycophytes including *Selaginella martensii* (*S. martensii*) *and Lycopodium squarrosum* (*L. squarrosum*)[27], as well as in the moss *Physcomitrella patens* (*P. patens*) —These findings suggest that key mechanisms underlying NPQ regulation by phosphorylated proteins may be conserved across broader plant lineages, but have not yet been identified in *Arabidopsis*. In *O. sativa*, STN8/PBCP-mediated CP29 phosphorylation enhances qE[26], though the underlying mechanism remains elusive. In contrast, P-CP24 in lycophytes actively drives qT formation[27], with its regulatory enzymes remaining uncharacterized. In *P. patens*, light-induced phosphorylation of CP24 has been observed and was dependent on STN8 kinase activity, though its physiological role remains uncharacterized. Furthermore, mass spectrometry analyses have identified phosphorylation events in CP29, PsbS and Thr42 of the CP24 chloroplast transit peptide in *A. thaliana*[28-30]; however, these modifications were minimal and had no significant impact on qE[26].

Beyond qE in PSII, an alternative photoprotective mechanism involves spillover — the transfer of excitation energy from PSII to PSI for dissipation—which reduces photodamage and enhances plant adaptation to high-light stress[6,31]. Energy dissipation by PSI is also supported by LHCSR1-dependent fluorescence quenching in *Chlamydomonas reinhardtii* (*C. reinhardtii*), where energy transfer from LHCII to PSI is facilitated for dissipation[32]. This mechanism requires the formation of PSII-PSI megacomplexes (mc1), which contain~50% of PSII in *A. thaliana*[6] and are enriched in CP24. Functional studies show that mc1 facilitates energy transfer from PSII to PSI even when PSII is closed, thereby directly contributing to photoprotection[6]. Cryo-EM studies of red algae mc1 (PBS-PSII-PSI-LHCI) demonstrate that CP47 interacts with PsaO through hydrophobic interactions, thereby positioning it adjacent to PSI[33]. Chl *a*617 within CP47 is proposed as a key energy transfer site between PSII and PSI[33]. Previous work demonstrated that *B. incana* preferentially channels energy to CP47 over CP43, creating a substantial energy reservoir at this site[34]. Given CP47's strategic location with in mc1 and its capacity to store excitation energy, spillover likely contributes to the distinctive photoprotection mechanism in *B. incana*. Importantly, CP24 binds CP47 via CP29 within this supercomplex[35], raising the possibility that HL-induced P-CP24 regulates spillover — a mechanism previously unreported in other angiosperms.

B. incana exhibits several exceptional photoprotective traits, including preferential energy transfer to CP47[34,36], rapid zeaxanthin synthesis[36], and robust tolerance to HL stress[37]. Despite its physiological uniqueness, the molecular basis of these adaptations remains poorly defined. Here, we integrated phosphoproteomics with physiological and biochemical analyses to systematically elucidate the molecular mechanisms underlying HL adaptation in *B. incana*. We identified extensive phosphorylation of CP24, mediated by a distinct kinase/phosphatase system separate from that regulating LHCII

phosphorylation. Functional characterization revealed that P-CP24 enhances qE specifically within PSI-PSII megacomplexes under HL conditions. We propose that CP24 functions as a molecular switch, dynamically tuning energy flux into and out of CP47 via changes in its phosphorylation state, thereby optimizing photoprotection in *B. incana*.

Results

Superior photoprotection and PSII stability of *B. incana* under HL conditions compared to *A. thaliana*

To compare the photoprotective capacity of *B. incana* and *A. thaliana*, we first assessed visible *Fv/Fm* and NPQ using a chlorophyll fluorescence imaging (CF-imager). Under normal physiological conditions, where *Fv/Fm* values were maintained above 0.8 for both species (Fig.1a), *B. incana* exhibited significantly higher NPQ levels compared to *A. thaliana* (Fig.1b). This observation suggests that *B. incana* has an enhanced capacity for dissipating excess light energy as heat under standard growth conditions. Consistently, Dual-PAM measurements revealed that *B. incana* exhibited both stronger NPQ induction under HL and faster NPQ relaxation compared to *A. thaliana* (Fig.1c, d). These findings demonstrate that *B. incana* possesses a superior capacity to rapidly initiate and complete the NPQ response, facilitating efficient adaptation to dynamically changing light conditions. To further dissect light energy utilization, we performed partitioning analysis of PSII-absorbed energy via Dual-PAM measurements of steady-state light response curves. When light intensity exceeded 500 μmol photons m^{-2} s^{-1}, *B. incana* showed a higher quantum yield of regulated non-photochemical quenching (Y(NPQ)) than *A. thaliana* (Fig.1e), indicating enhanced active regulation and thermal dissipation of excess energy. Conversely, *A. thaliana* maintained higher Y(NO) values across all light intensities (Fig.1f), reflecting greater energy loss as heat due to inefficient utilization or NPQ-independent dissipation. Since NPQ is quantified as the ratio of Y(NPQ) to Y(NO), *B. incana* exhibited consistently higher NPQ levels than *A. thaliana* (Fig.1g), which aligns with imaging-PAM measurements (Fig.1a, b). These findings collectively demonstrate the superior photoprotective capacity of *B. incana*. The enhanced photoprotection in *B. incana* correlates with sustained higher PSII activity. This is evidenced by faster electron transport rate (Fig.1i) and increased quantum yield of PSII (Fig.1j) under high-light conditions. The relatively higher ETR(II) and Y(II) values indicate that *B. incana* maintains superior photosynthetic performance even when exposed to excessive irradiance.

Unique HL-dependent CP24 phosphorylation occurs in *B. incana*

Given the established role of thylakoid membrane protein phosphorylation in photoprotection[11,12,26,27], We compared PSII protein phosphorylation patterns between *B. incana* and *A. thaliana* under growth light (GL) and HL conditions (30, 60, and 90 min after GL-to-HL transfer) using anti-P-Thr immunoblotting (Fig.2a). Under GL conditions, both species exhibited basal phosphorylation of PSII core proteins (D1, D2), inner antenna CP43, and LHCII polypeptides (Fig.2a, GL). Upon HL treatment, D1, D2, and CP43 showed significant increases in phosphorylation in both species, while LHCII phosphorylation progressively declined with prolonged stress (Fig.2a, HL30 to HL90). Notably, *B. incana* specifically exhibited a novel HL-dependent phosphoprotein band corresponding to the size of CP24, which was absent in *A. thaliana* (Fig.2a, HL30 to HL90). This finding contrasts with previous reports that have exclusively documented P-CP24 in lycophytes and mosses[27,38]. This is the first observation of such a phosphorylated CP24-like protein in a dicot species. Parallel anti-CP24 immunoblotting confirmed stable CP24 protein levels during HL stress (Fig.2a), indicating that the observed changes were specific to phosphorylation rather than protein abundance.

To map the phosphorylation sites on P-CP24, we performed thylakoid membrane phosphoproteomics. The analysis identified Ser−24 (located in the chloroplast transit peptide) and Ser-53, Thr−178, Thr−206 (all in the mature protein) as phosphorylation sites (Fig.2b and Supplementary Table 1). Among these, only Thr−178 showed HL-dependent upregulation (Fig.2c), suggesting its critical role in the HL response. Sequence alignment revealed that Thr−178 is conserved among *B. incana, S. martensi* and *A. thaliana* (Fig.2d), implying that differential phosphorylation patterns likely arise from kinase specificity rather than substrate sequence variation. This conservation underscores the potential functional significance of this site across different plant species, despite the unique HL-dependent phosphorylation observed in *B. incana*.

CP24 phosphorylation/dephosphorylation is catalyzed by enzymes other than those for LHCII

To characterize the HL-dependent phosphorylation dynamics of P-CP24 in *B. incana*, we analyzed PSII peptide phosphorylation patterns under diverse light conditions (Fig.3a). Plants were subjected to: (1) dark incubation for 12 h (D12); (2) red light (RED) preferentially exciting PSII for 2 h; (3) high light (HL, 2 h); (4) far-red light (FR) preferentially absorbed by PSI after HL treatment; and (5) dark recovery for 15 min, 1 h, 2 h, and 6 h after HL exposure. Under dark conditions, D1, D2, CP43, and LHCII exhibited basal phosphorylation (Fig.3a, D12). PSII-light exposure for 2 h enhanced phosphorylation of D2 and LHCII compared to D12 (Fig.3a, PSII). HL treatment for 2 h further increased D1 and D2 phosphorylation relative to PSII-light and dark conditions (Fig.3a, HL), while LHCII phosphorylation was markedly reduced (Fig.3a, HL). Notably, a distinct P-CP24 band emerged under HL (Fig.3a and Supplementary Fig 1a, HL), rapidly reaching maximal phosphorylation levels (Supplementary Fig.1a, b). To assess PQ pool oxidation effects, PSI-light treatment (15 min) after HL stress slightly decreased PSII core subunit phosphorylation but markedly reduced LHCII phosphorylation (Fig.3a, PSI). In contrast, the P-CP24 band persisted under PSI-light conditions (Fig.3a, PSI). During dark recovery, LHCII phosphorylation rapidly increased, reaching GL-equivalent levels within 15 min (Fig.3a, Dark), whereas P-CP24 signals progressively declined and disappeared after 6 h (Fig.3a, Dark and Supplementary Fig.1b). These results demonstrate that CP24 phosphorylation occurs independently of the systemic light response, being rapidly induced by HL conditions but progressively dephosphorylated in darkness. This dynamic phosphorylation pattern exhibits an inverse relationship compared to that of LHCII.

Given that CP24 exhibited a phosphorylation pattern more closely resembling PSII core proteins than LHCII (Fig.3a), we assessed recombinant PBCP (rPBCP) — mediated dephosphorylation of PSII components. Incubation with rPBCP for 10 min resulted in complete dephosphorylation of P-CP24 and significant dephosphorylation of PSII core proteins (D1/D2), whereas substantial P-LHCII remained even after 15 min (Fig.3b). Considering the antagonistic roles of STN8 (kinase) and PBCP (phosphatase) in PSII core phosphorylation dynamics[24], we attempted to express *B. incana* STN8 kinase. Unfortunately, active STN8 could not be obtained. We therefore performed multiple sequence alignments of STN7 and STN8 kinases from *B. incana* and *A. thaliana*. While full-length STN7 exhibited high conservation (Supplementary Fig.2), STN8 displayed notable variation in its N-terminal stroma-binding domain but retained strong conservation in the C-terminal catalytic domain (Supplementary Fig.3). These structural differences suggest that STN8's broad substrate specificity — including CP24 phosphorylation—may arise from its unique stroma-binding domain architecture. These findings demonstrate that CP24 phosphorylation and dephosphorylation are catalyzed by distinct enzymatic mechanisms from those governing LHCII.

An in vitro assay for CP24 phosphorylation

To elucidate the mechanisms underlying CP24 phosphorylation regulation, we established an in vitro system to recapitulate this process. Functional chloroplasts were exposed to HL under ATP-depleted or ATP-supplemented conditions, with or without dark incubation. Immunoblotting with anti-P-Thr antibody revealed that P-CP24 formation required both HL illumination and ATP supplementation, as evidenced by the absence of P-CP24 bands in dark controls and ATP-depleted conditions (Fig.3c). To determine the subcellular localization of the CP24 kinase, we compared CP24 phosphorylation levels in functional chloroplasts versus isolated thylakoid membranes under HL conditions. Notably, P-CP24 abundance was comparable between these two fractions (Fig.3d), suggesting that the CP24 kinase is a thylakoid membrane-associated protein.

Next, we aim to identify kinase inhibitors capable of suppressing CP24 phosphorylation in vitro, as this is essential for elucidating the functional substantial CP24 phosphorylation. we tested kinase inhibitors targeting distinct signaling pathways. Chloroplast extracts were treated with three inhibitors under HL conditions in the presence of ATP: k252a (50 μM), a broad-spectrum serine/threonine protein kinase inhibitor; U0126 (30 μM), a mitogen-activated protein kinase (MAPK) inhibitor; and W7 (100 μM), a Ca^{2+}-dependent protein kinase inhibitor. Immunoblotting revealed that only k252a significantly suppressed CP24 phosphorylation (Fig.3e), while U0126 and W7 showed no inhibitory effect. Dose-response experiments further determined the optimal inhibitory concentration of k252a for CP24 phosphorylation in chloroplasts (40 mg mL^{-1} chloroplasts final chlorophylls concentration) as 20 μM (Supplementary Fig.4). These findings identify CP24 kinase as a serine/threonine protein kinase, consistent with the phosphorylation mechanisms governing PSII core, CP29 and LHCII.

To elucidate how redox states of the PQ pool and cytochrome b_6f (Cyt b_6f) complex regulate CP24 phosphorylation, we treated chloroplasts with either 3-(3,4-dichlorophenyl)−1,1-dimethylurea (DCMU; 100 μM) or 2,5-dibromo-6-isopropyl-3-methyl−1,4-benzoquinone (DBMIB; 200, 400, or 800 μM). DCMU completely abolished CP24 phosphorylation (Fig.3f), while DBMIB exhibited concentration-dependent inhibition: partial suppression at 200 – 400 μM and complete inhibition at 800 μM (Fig.3f). Given that DCMU decreases and DBMIB increases the redox state of PQH_2, these results suggest that the CP29 kinase is activated by the reduction of PQH_2 and/or the cytochrome b_6/f complex.

Native localization of phosphorylated CP24 is predominant in mc1 (PSII-PSI megacomplexes)

To elucidate the native localization of P-CP24, we performed two-dimensional large pore blue-native/SDS-PAGE (2D lp-BN/SDS-PAGE) analysis on thylakoid membranes solubilized with β-dodecyl maltoside (β-DM) from *B. incana* exposed to GL or HL. Immunodetection using anti-P-Thr or anti-CP24 antibodies in the second dimension revealed that P-CP24 was exclusively detected in HL-treated plants, predominantly localized to LHCII monomers and LHCII assembly, with minimal association with LHCII supercomplexes (Fig.4a, b). Parallel immunoblotting with anti-CP24 antibody confirmed the co-localization of P-CP24 and CP24 in identical 2D lp-BN/SDS-PAGE spots (Fig.4b). This assignment was further validated by MALDI-TOF-TOF mass spectrometry, which assigned the phosphoprotein isolated from both LHCII assemblies and monomers as CP24 (Supplementary Fig.5a, b).

The absence of apparent P-CP24/CP24 signal in any supercomplexes (Fig.4a, b) prompted us to hypothesized the β-DM might disrupt protein-protein interactions within supercomplexes due to its strong detergent properties. To address this, we employed digitonin, a milder detergent, for solubilizing stroma-exposed thylakoid membranes[39]. Based on previous reports[40], the first-dimension PAGE bands (Fig.4c, d) were assigned as: (1) PSII-PSI megacomplexes I (mc1), (2) PSI megacomplexes (PSI and PSII mixed megacomplexes), (3) PSI-LHCII supercomplex, (4) PSI complexes, (5) PSII core dimer (C2)/ATPase complex, (6) PSII core monomers, (7) LHCII assemblies, (8) LHCII trimers, and (9) LHCII

monomers. Immunoblotting revealed that P-CP24 and CP24 predominantly localized to mc1, with apparent distribution in LHCII assemblies and monomers, and minor signals in PSII core dimer (C2)/ATPase complex and PSI megacomplexes (Fig.4c, d). These findings demonstrate that P-CP24 is natively enriched in the mc1 complex, specifically within the stroma-exposed regions of PSI-enriched thylakoid membranes.

In addition, we further characterized PsbS — a protein known to play a critical role in high-light-induced NPQ and undergo extensive phosphorylation in Norway spruce *Picea abies* (*P. abies*). We found it primarily localizes to the LHCII monomer (Fig.4a-d); however, Western blotting failed to detect its phosphorylated isoforms in *B. incana*. Notably, under high-light conditions, PsbS abundance in the mc1 decreased significantly (Fig.4c, d), implying it is unlikely to participate in the spillover process.

CP24 phosphorylation enhances NPQ in *B. incana*

To investigate the physiological role of CP24 phosphorylation, we employed k252a — a validated inhibitor of CP24 phosphorylation (Fig.3e and Supplementary Fig.4) — as a pharmacological tool, given the lack of a kinase mutant specifically targeting CP24 phosphorylation in *B. incana*. Considering *B. incana* exhibits exceptionally robust photoprotective capacity under HL[34,36,37], we hypothesized that P-CP24 may contribute to the enhanced NPQ observed under HL (Fig.1c). To test this, we evaluated NPQ dynamics in chloroplasts exposed to HL (1,000 μmol photons m^{-2} s^{-1}) under three experimental conditions: (1) wild-type (WT) with ATP (WT + ATP); (2) WT with ATP and k252a (WT + ATP + k252a); and (3) WT without ATP or k252a (control: WT). Following the first light-dark cycle (16 min actinic light/10 min dark), NPQ values were comparable between k252a-treated (0.55 ± 0.03) and untreated controls (0.53 ± 0.02), but increased by ~ 33% in +ATP samples (0.74 ± 0.04; Fig.5a). This difference progressively amplified across three light cycles, with the +ATP group exhibiting an NPQ value of 1.02 ± 0.03 after the third cycle (Fig.5a), indicating enhanced CP24 phosphorylation under repeated HL stress. Notably, dark relaxation kinetics were ~1.6-fold faster in k252a-treated samples versus + ATP controls after the third cycle (Fig.5a). To exclude photoinhibition as the underlying cause, we measured the *Fv/Fm*. Higher *Fv/Fm* values in + ATP samples versus k252a-treated controls (Fig.5b) confirmed that accelerated dark relaxation was not due to photodamage. Given that NPQ alleviates photoinhibition by scavenging reactive oxygen species (ROS), we employed Singlet Oxygen Sensor Green™ to quantify singlet oxygen ($^1O_2$) production. As predicted, k252a treatment significantly increased $^1O_2$ levels (Fig.5c), linking CP24 phosphorylation to enhanced photoprotection via ROS scavenging.

To investigate whether phosphorylated PSII core proteins contribute to NPQ regulation in *B. incana*, given that its phosphorylation levels are similarly elevated under HL conditions and are suppressed by k252a. We analyzed chloroplasts isolated from *B. incana* plants exposed to systemic light treatment. Immunoblotting revealed markedly enhanced LHCII phosphorylation under PSII-light conditions, whereas PSI-light exposure significantly reduced phosphorylation of all PSII core proteins (Fig.5d). Contrary to expectations, NPQ measurements showed no significant differences among the light conditions (Fig.5e). This observation was further supported by analyses of *A. thaliana stn7/8* double mutants, where PSII core phosphorylation was nearly abolished (Fig.5f) yet NPQ levels remained comparable to wild-type (WT) plants (Fig.5g). These findings demonstrate that PSII core protein phosphorylation does not drive NPQ enhancement, a conclusion with potential cross-species conservation.

To assess whether P-CP24 modulates NPQ via zeaxanthin (Zea) and lutein (Lut) accumulation, we performed HPLC-based quantification of carotenoids. Contrary to expectations based on their established quenching roles[19], Zea and Lut levels showed no significant differences between WT + ATP + k252a and

WT + ATP samples (Supplementary Fig.6a-d), suggesting NPQ enhancement is independent of these carotenoids. To further dissect NPQ contributions, we manipulated Zea epoxidase (ZEP) activity by varying Na-ascorbate (Asc) availability in chloroplasts — a cofactor essential for Zea synthesis (Supplementary Fig.6e). Under Asc-deficient conditions (- Asc), NPQ levels were significantly reduced compared to Asc supplemented controls (Supplementary Fig.6f, - Asc vs + Asc). Notably, ATP addition to - Asc samples (-Asc + ATP) partially restored NPQ but remained below + Asc levels (Supplementary Fig.6f, - Asc + ATP vs + Asc). These results demonstrate that while both P-CP24 and Zea contribute additively to NPQ enhancement, their effects are mechanistically independent. Specifically, the NPQ increase in + Asc + ATP samples relative to + Asc controls (Supplementary Fig.6f, C2) reflects P-CP24 — specific contributions beyond Zea/Lut-mediated quenching (Supplementary Fig.6f, C1) —a feature unique to *B. incana* under HL stress.

HL-dependent CP24 phosphorylation is not involved in the state transition-like function

Previous studies have demonstrated that HL-induced CP24 phosphorylation in lycophytes enhances qT under HL conditions[27], suggesting a potential role for P-CP24 in mediating energy distribution to PSI. To assess whether P-CP24 exerts similar functions in *B. incana*, we evaluated state transitions by applying FR under HL to induce excitation redistribution from PSII to PSI. Contrary to expectations, FR light induced only marginal changes in *Fm'/Fm* under HL (Fig.6a), indicating that CP24 phosphorylation does not regulate energy distribution between photosystems in *B. incana*. This conclusion was further supported by analyzing NPQ dark relaxation kinetics. We monitored NPQ induction at GL (50 μmol photons m^{-2} s^{-1}) and HL (800 μmol photons m^{-2} s^{-1}), followed by dark relaxation (Fig.6b). Semi-logarithmic plots of dark relaxation kinetics revealed biphasic decay patterns, with rapid qE relaxation and slower qT decay, while residual NPQ after 20 min in darkness was quantified as qI (Fig.6c). Quantitative analysis of NPQ components demonstrated that HL significantly increased qE and qI (Fig.6d), while qT fraction was reduced under HL compared to GL (Fig.6d). This dissociation between CP24 phosphorylation and qT enhancement in *B. incana* contrasts with observations in *S. martensii*[27], despite similar HL-induced phosphorylation patterns in both species. This divergence suggests that the functional role of CP24 phosphorylation may be shaped by species-specific light adaptations. Notably, *B.incana* is a sun-adapted species with a high chlorophyll *a/b* ratio (3.3) (Fig.6e), whereas *S. martensii* is shade-adapted and exhibits a lower chlorophyll *a/b* value (2.3–2.7)[41].

Previous studies in *C. reinhardtii* and barley have demonstrated that P-CP29 translocates from PSII to PSI under HL conditions[42,43]. To investigate whether CP24 phosphorylation induces a similar suborganellar relocation in *B. incana* to balance energy distribution between the two photosystems, we performed SDS-PAGE analysis on gradient-separated thylakoid membrane fractions from plants grown under GL or HL stress. Immunoblotting revealed that PSII core proteins were primarily localized to grana stacks, whereas PSI and ATP synthase were predominantly distributed in stroma lamellae, with minor PSI fractions in grana membranes (Fig.6e). Consistent with the functional specialization of photosystems, the stromal fraction enriched in PSI exhibited a significantly higher chlorophyll *a/b* ratio (5.5) than the grana fraction (2.5) enriched in PSII (Fig.6e), as PSI predominantly contains chlorophyll *a*, whereas PSII is enriched in chlorophyll *b*[44]. Although anti-P-Thr immunodetection confirmed HL-induced CP24 phosphorylation (Fig.6e), anti-CP24 immunoblotting showed no significant changes in CP24 protein levels between GL and HL conditions, regardless of suborganellar localization (Fig.6e, grana vs. stroma membranes). These findings demonstrate that P-CP24 occurs in situ without translocation between grana and stroma membranes.

CP24 phosphorylation promotes energy transfer from CP47 to PSI under HL

A notable spectral distinction of *B. incana* compared to *A. thaliana* is the significantly enhanced fluorescence emission peak at 695 nm — originating from CP47 — relative to the 685 nm peak associated with CP43, as revealed by 77K fluorescence emission spectra (Fig.7a). This spectral shift indicates a preferential energy transfer to CP47 in *B. incana*, in contrast to the preferential transfer to CP43 observed in *A. thaliana*[36]. Given that P-CP24 is mainly localized in mc1 — a megacomplexes facilitating PSII-to-PSI energy transfer for photoprotection — and structurally positioned between CP47 and PSI[6,35], we hypothesized that P-CP24 mediates excitation energy routing from CP47 to PSI in mc1. To test this, we measured time-resolved fluorescence spectra at 77K using thylakoid membranes from GL- or HL-treated *B. incana* and *A. thaliana*. HL treatment significantly shortened average fluorescence lifetimes (685 – 716 nm) in *B. incana* (Fig.7b) but not in *A. thaliana* (Supplementary Fig.7a), indicating accelerated energy dissipation at CP47 (≈ 695 nm) via PSI transfer or in situ quenching in *B. incana*. Global analysis of fluorescence decay kinetics identified four components (Fig.7c and Supplementary Fig.7b): The first component (307-372 ps) showed PSII-to-PSI energy transfer and LHCII dissipation (conserved in both species). The second (1.1 ns) and third component (2.6 ns) indicated energy transfer to a putative quenching site (similar spectral patterns; enhanced PSI-region amplitudes under HL). The fourth component (5.1-5.4 ns) is associated with fluorescence emitted from the final energy traps in both PSII and PSI. Notably, *B. incana* exhibited reduced PSII (695 nm) amplitude under HL compared to GL, while *A. thaliana* showed no change (Fig.7c, 5.3-5.5 ns). This demonstrates that HL-induced P-CP24 facilitates energy dissipation or transfer from CP47 to PSI under high-light conditions in *B. incana*.

To delineate the action site and mechanism of P-CP24 in enhancing NPQ, we isolated thylakoid membranes from *B. incana* grown under GL or HL conditions, performed clear-native (lp-CN)-PAGE separation of P-CP24-containing complexes (Supplementary Fig.8), and measured their fluorescence lifetimes. Room-temperature fluorescence decay analysis revealed that the mc1 (containing PSII-PSI complexes) under HL exhibited a significantly shortened 695 nm fluorescence lifetime compared to GL (Fig.7d). In contrast, PSI-megacomplexes (containing simple mixture of PSII and PSI) with minimal P-CP24 content (Fig.4d) showed no light-dependent changes in the fluorescence lifetime (Fig.7e). Although LHCII assemblies and monomers contained abundant P-CP24, their 695 nm fluorescence lifetimes remained unchanged under both light conditions (Fig.7f, g). These results demonstrate that P-CP24 does not mediate in situ energy dissipation at the PSII level but instead enhances PSII-to-PSI energy transfer to dissipate preferentially accumulated CP47 energy, thereby contributing to photoprotection.This further indicates that the reduction in 695 nm fluorescence lifetime of *B. incana* within the fourth lifetime component (5.1–5.4 ns) of DAS spectra (Fig.7c) is caused by energy spillover from CP47 to PSI.

Discussion

The phosphoproteins of the thylakoid membrane, as detectable by western blotting (WB), are dominated by PSII proteins such as CP43, D2, and D1, along with LHCII, and the small transmembrane protein PsbH[45,46]. Among these, PsbH maintains stable phosphorylation levels under both control and HL conditions[45], suggesting a constitutive rather than regulatory role. In contrast, lineage-specific phosphorylated proteins have been identified across diverse plant lineages: P-CP24 is associated with enhanced qE in the sun-adapted dicotyledonous *B. incana* — and with qT in shade-adapted lycophytes under HL (Supplementary Fig.9)[27]; similarly, P-CP29 correlates with qE in monocots like *O. sativa* (Supplementary Fig.9)[26]. While mass spectrometry has identified phosphorylation events in other photosynthetic membrane proteins[29,47,48], these modifications are typically low-abundance and show negligible contribution to qE enhancement[26]. Here, we report for the first time that CP24 in the

angiosperms *B. incana* undergoes substantial phosphorylation, a phenomenon previously observed only in early land plants such as lycophytes and mosses, suggesting either evolutionary conservation or convergent adaptation, This finding further implies that CP24 phosphorylation may represent a conserved regulatory mechanism within the photosynthetic machinery of land plants, potentially preserved across angiosperms but yet to be widely recognized. We further investigated whether HL-induced reversible phosphorylation of CP24 in *B. incana* is mediated by the same enzymatic machinery known to regulate LHCII phosphorylation. Finally, we assessed how CP24 phosphorylation and the associated remodeling of energy transfer pathways contribute to enhanced photoprotection in *B. incana*.

Unique regulation of CP24 phosphorylation in *B. incana*

In angiosperms, STN7 and STN8 Ser/Thr protein kinases serve as master regulators of PSII protein phosphorylation within the thylakoid membrane, exhibiting distinct redox sensitivities: reduced thioredoxin inhibits STN7 but not STN8[13]. Our functional characterization reveals that the CP24 kinase localizes to the thylakoid membrane (Fig.3d) and is potently inhibited by k252a (Fig.3e and Supplementary Fig.4a, b), a broad-spectrum Ser/Thr protein kinase inhibitor. While *B. incana* shares canonical regulation in LHCII phosphorylation with other angiosperms — positively regulated by reduced PQ (Fig.3a: PSI) and negatively regulated by reduced thioredoxin (Fig.3a: HL) — the CP24 phosphorylation cascade displays unique features. Notably, CP24 phosphorylation is activated by reduced PQ and Cyt b_6f in vitro (Fig.3f), similar to STN7-mediated LHCII phosphorylation. However, unlike STN7 substrates, CP24 phosphorylation is enhanced under HL conditions, where reduced thioredoxin would normally suppress STN7-mediated phosphorylation (Fig.2a: HL; Fig.3a: HL; Supplementary Fig.1Fig.1). This inverse redox response may suggest that CP24 phosphorylation is predominantly mediated by STN8 rather than STN7. The STN8 exhibits an expanded substrate specificity, primarily targeting structurally distinct PSII core proteins and CP29[23,45], which — similar to CP24 — undergo enhanced phosphorylation under HL stress. The conserved Thr−178 phosphorylation site across *A. thaliana*, *S. martensii*, and *B. incana* (Fig.2d) indicates that substrate sequence variation is not the primary determinant of CP24 phosphorylation patterns. Sequence alignment analyses reveal significant divergence in the N-terminal substrate-binding domain of STN8 between *A. thaliana* and *B. incana* (Supplementary Fig.3), which contrasts with the near-complete sequence conservation observed in STN7 (Supplementary Fig.2). These differences may underlie the expanded substrate repertoire of STN8 in *B. incana*. Functionally, STN8 and PBCP form a tightly coupled antagonistic pair. Our data demonstrate that recombinant rPBCP efficiently dephosphorylates PSII core protein and CP24, but shows markedly reduced activity toward P-LHCII (Fig.3b). This hierarchy of dephosphorylation efficiency aligns with previous studies[23,24]. Furthermore, this substrate hierarchy supports the notion that LHCII is not the primary physiological target of PBCP, whereas CP24 and other PSII core proteins represent key substrates for dynamic phosphorylation-dephosphorylation cycles under HL stress.

CP24 phosphorylation mediates enhanced NPQ via spillover mechanism independent of xanthophyll cycle

NPQ, a critical photoprotective mechanism that dissipates excess light energy as heat, is primarily localized to LHCII trimers[19,49,50] and monomeric antennae such as CP24, CP26, and CP29[49,51-53]. These components are differentially regulated by xanthophyll cycle pigments and conformational changes within the antenna complexes[53]. While LHCII-mediated NPQ relies on Zea accumulation via the xanthophyll cycle and conformational rearrangements induced by Zea binding, monomeric antennae-initiated NPQ requires coordinated enrichment of Zea, Lut, and carotenoid cation radicals[19,54], highlighting divergent molecular dependencies between these two pathways. Strikingly, *B. incana*

exhibits an exceptionally strong NPQ response: while HL-induced Zea accumulation initially elevates NPQ (Supplementary Fig.6a and f: + Asc vs - Asc), a subsequent phase of quenching enhancement occurs independently of further pigment accumulation (Supplementary Fig.6a-d and f: + Asc vs + Asc +ATP). This decoupling reveals an unanticipated regulatory layer, wherein P-CP24 specifically drives NPQ potentiation without concurrent increases in zeaxanthin or lutein levels. These findings challenge the prevailing paradigm that NPQ enhancement is tightly coupled to xanthophyll cycle pigment dynamics, suggesting instead that antenna protein phosphorylation — particularly at CP24 — may serve as a direct switch for advanced quenching states. This raises a critical question: whether phosphorylated monomeric antenna proteins (CP24) are truly energy dissipation sites? Our room-temperature fluorescence decay measurements reveal a significant 695 nm lifetime decrease exclusively within the mc1 complex (Fig.7d), despite the presence of P-CP24 in both LHCII assemblies (Fig.7f) and monomers (Fig.7g). This spatial mismatch — where P-CP24 is present but lifetime reduction occurs only in mc1 — strongly suggests its exclusion from direct PSII-level quenching. Interestingly, P-CP24 is predominantly localized to the mc1 (Fig.4d) where spillover occurs, consistent with its functional role in energy transfer within mc1 and bypasses the xanthophyll cycle-dependent pathway. Crucially, PSI and PSII mixed megacomplexes (PSI-megacomplexes) lack the characteristic 695 nm lifetime reduction (Fig.7e), underscoring that P-CP24-mediated NPQ enhancement requires physiological spillover rather than simple protein proximity. Furthermore, despite substantial phosphorylation of PSII core components in the mc1 complex under HL conditions, comparative analyses of systemically light-treated *B. incana* (Fig.5d, e) and HL-exposed *A. thaliana* reveal no corresponding NPQ alterations (Fig.5f, g). This dissociation between PSII core phosphorylation and NPQ modulation strongly implicates P-CP24 as the primary molecular determinant of spillover initiation, rather than generalized PSII modifications. Notably, our phosphoproteomic analysis also revealed elevated phosphorylation of PsbS (Supplementary Table 2), a protein critically implicated in NPQ. However, its phosphorylation level was very weak, as evidenced by its undetectability via WB (Fig.4d). Previous reports have shown that heavily phosphorylated PsbS was exclusively detected in *P. abies* (Supplementary Fig.9), where its phosphorylation status specifically correlates with qH induction rather than qE activation[55]. In contrast, under HL conditions, PsbS protein levels were markedly reduced in the mc1 complex of *B. incana* (Fig.4c vs d), a spatial distribution pattern that sharply contrasts with a proposed regulatory role in spillover. Importantly, although PsbS phosphopeptides also were identified in *A. thaliana* through phospho-enrichment techniques[48], their in vitro phosphorylation under high-induction conditions failed to enhance qE in *A. thaliana* [26]. Collectively, these observations indicate that the PsbS phosphorylation is unlikely to underlie phosphorylation-regulated spillover.

Here, we report P-CP24 in the angiosperm *B. incana*, revealing a previously underappreciated NPQ mechanism that may be broadly conserved yet overlooked in terrestrial plants. Unlike previous observations in lycophytes, where P-CP24 is associated with enhanced qT[27], our findings demonstrate that P-CP24 in *B. incana* enhances qE in an mc1-dependent manner. This functional divergence likely reflects their distinct evolutionary adaptations and ecological niches. Lycophytes, which typically grow in shade acclimation, endure high excitation pressure on PSII even under low-light conditions. Consequently, they may rely on state transitions to mitigate fluctuating light environments under limited strong light exposure; however, a spillover function of P-CP24 in lycophytes cannot be excluded. In contrast, *B. incana*, which is adapted to heliophilous conditions in temperate desert margins, frequently encounters light intensities of up to 2, 000 μmol photons m^{-2} s^{-1}. Such extreme light exposure has driven the evolution of multiple photoprotective mechanisms in this species.

Building upon structural insights from You et al., who elucidated the organization and energy transfer pathways in red algal PSII–PSI–LHC megacomplexes[33], we propose a model (Fig. 8) that illustrates how P-CP24 contributes to NPQ via spillover under HL in this desert-adapted angiosperm *B. incana*. The energy transfer pattern in *B. incana* differs from that of typical angiosperms: energy is preferentially directed to the low-energy antenna protein CP47 rather than the high-energy CP43 (Fig.8a). This redistribution generates a distinct energy accumulation peak at 695 nm (Fig.8b), constituting a photoprotective strategy by limiting excitation transfer to the high-energy PSII reaction center. Notably, this unique energy distribution may be driven by conformational changes within the photosynthetic machinery — potentially induced or stabilized by P-CP24 phosphorylation. Furthermore, P-CP24 localized within the mc1 facilitates accelerated energy transfer from CP47 to PSI for quenching (Fig. 8c), thereby significantly reducing excitation pressure on the PSII reaction center under HL conditions. This dynamic reorganization likely reflects both structural rearrangements and functional modulation mediated by P-CP24, ultimately ensuring robust photoprotection (Fig.8d).

We conclude that the modified energy transfer dynamics under moderate light conditions, together with P-CP24-mediated spillover regulation under HL, synergistically confer *B. incana* with exceptional photoprotective capacity. These findings reveal a previously unrecognized adaptive strategy in terrestrial plants and significantly expand our current understanding of NPQ mechanisms. Moreover, this study highlights the vast potential of exploring natural variation to uncover novel photoprotective strategies, which may lead to the identification of new engineering targets for improving crop yield and biomass production.

Methods

Plant materials and growth condition

Seeds of *B. incana* and *A. thaliana* were imbibed in the dark for 2 days at 4 °C to ensure synchronized germination. Subsequently, the seeds were sown and transferred to growth chambers (100 μmol photons m^{-2} s^{-1}, and 12 h light/12 h dark at 22 °C, 50 - 70% relative humidity) for the first 2 weeks. Then, the two-week-old seedlings were transferred and cultured in greenhouse at 23 °C with growth light of 100 μmol photons m^{-2} s^{-1}. All analyses were performed with 4-week-old leaves.

Membrane isolation, SDS-PAGE and immunoblotting

Thylakoid membranes used for in vivo phosphorylation experiments were isolated as described previously in the presence of NaF to inhibit thylakoid proteins dephosphorylation[56]. Functional chloroplast/thylakoid used for in vitro phosphorylation experiments were isolated as described previously with slightly modified[57]. Briefly, 10 grams of *B. incana* leaves were rapidly homogenized using mortar and pestle in 10 mL of grinding buffer (GB) containing 0.4 M sorbitol, 5 mM EDTA, 5 mM EGTA, 5 mM $MgCl_2$, 10 mM $NaHCO_2$, 20 mM Tricine/NaOH (pH 8.4) and 0.5% (w/v) fatty acids-free BSA. The homogenate was filtered through 8 layers of cheesecloth, with a gentle hand pressure being applied in order to increase the final thylakoid yield. The suspension was centrifuged at 2600 g for 3 min at 4 °C, the supernatant was discarded and the pellet was resuspended in 2-3 mL of resuspending buffer (RB) containing 0.3 M sorbitol, 2.5 mM EDTA, 5 mM $MgCl_2$, 10 mM $NaHCO_3$, 20 mM HEPES (pH 7.6) and 0.5% (w/v) fatty acids-free BSA. The above resuspended material was then loaded on top of a Percoll step gradient developed with 4 mL of 10%, 3 mL of 30%, and 2 mL of 50% Percoll in RB and centrifuged at 8000g for 20 min. Functional chloroplasts were collected from the interphase between 30 and 50% Percoll, washed twice with RB. To obtain thylakoid membranes from functional chloroplasts, the chloroplasts were centrifuged at 2600 g for 3 minutes at 4 °C. Next, the resulting pellet was suspended

in 20 mL of hypotonic buffer (HB) containing 2.5 mM EDTA, 5 mM $MgCl_2$, 10 mM $NaHCO_3$, 20 mM HEPES (pH 7.6) and 0.5% (w/v) fatty acids-free BSA followed by placing on the ice for 20 minutes. The thylakoid membranes were collected by centrifugation at 2600 g for 3 min at 4 °C. Finally, the pellet was resuspended in a small volume (0.5 - 1 ml) of RB and the suspension was stored in ice in the dark for use. Grana membranes and stroma lamellae were prepared as described previously by stepwise centrifugation (Morosinotto et al., 2010). All successive steps mentioned above were carried out in the dark at 4 °C and all materials and buffers were precooled before use. The chlorophyll concentrations were calculated from the absorbances at 645 and 663 nm after extraction with 80% (v/v) acetone.

SDS-PAGE analysis was performed with 4% acrylamide stacking gel and 15% acrylamide resolving gel containing 6 M urea. For immunoblotting analysis, chloroplast or thylakoid proteins were loaded on SDS-PAGE and transferred to a nitrocellulose membrane. After blocking with 1% BSA, proteins were detected with the corresponding antibody from Agrisera (www. Agrisera. com). For detection of phosphoproteins, anti-P-Thr polyclonal antibody was used.

High light treatments and phosphorylation experiment in vivo and in vitro

High light conditions were provided by metal halide lamps with 20% blue light and 80% red ligh, and the light was filtered through a glass tray filled with cold water to avoid heat and UV effects.

For in vivo phosphorylation experiments, plants were dark-adapted for 12 h prior to light treatments, followed by exposure to red light (30 μmol photons m^{-2} s^{-1}) for 2 h or high light (1000 μmol photons m^{-2} s^{-1}) for 30 min、1 h、1.5 h、2 h and 2.5 h. After 2 h high light treatment, plants were subjected to either far-red light (6 μmol photons m^{-2} s^{-1}) for 15 min or directly transferred to darkness for 15 min, 1 h, 2 h, or 6 h. In vitro phosphorylation experiments were performed using functional chloroplasts/thylakoids isolated from plants acclimated to growth light conditions. The isolated chloroplasts/thylakoids were resuspended in reaction buffer containing 10 mM methylviologen, 0.5 mM ATP, and 15 mM sodium ascorbate (Asc), and exposed to high light (1000 μmol photons m^{-2} s^{-1}) for 30 min at a final chlorophyll concentration of 40 μg mL^{-1}. Thylakoid membranes were isolated from treated plants, and phosphorylation and dephosphorylation dynamics of target proteins were detected by western blotting using an anti-phosphothreonine (anti-p-Thr) antibody.

Pre-treatment and analysis of phosphoproteomics

For phosphoproteomic analysis, thylakoid membranes were isolated from 4-week-old leaves (approximately 60 μg Chl per sample). Each condition included two biological replicates for LC-MS/MS. Proteins were extracted from thylakoid membrane pellets using a lysis buffer containing 2% SDS, 100 mM Tris-HCl (pH 8.0), 100 mM EDTA, 10 mM TCEP, 1× protease inhibitor cocktail, 1× phosphatase inhibitor cocktail, and PMSF, with a membrane pellet-to-lysis buffer ratio of 1:4 (w/v). Samples were sonicated on ice for 60 minutes at 4°C, followed by centrifugation to collect the supernatant. Proteins were precipitated by adding five volumes of pre-chilled acetone (−20°C) and incubating overnight at −20°C. After centrifugation at 4°C, the supernatant was discarded, and the pellet was washed twice with ice-cold 90% acetone. The precipitated proteins were dissolved in 8 M urea, and the protein concentration was determined using a BCA protein assay kit (Thermo, A55864). For digestion, 1 mg of total protein was aliquoted, reduced with TCEP to a final concentration of 10 mM, and alkylated with chloroacetamide (CAA) to a final concentration of 50 mM. The sample was incubated at 37°C for 30 minutes with shaking at 650 rpm. The urea concentration was then diluted to less than 1 M by adding 100 mM ammonium bicarbonate solution. Trypsin was added at an enzyme-to-substrate ratio of 1:25, and the sample was incubated overnight for digestion. The reaction was terminated by adding trifluoroacetic acid (TFA) to a final concentration of 2%, bringing the pH below 3. Peptides were desalted using C18 cartridges and

quantified using a peptide quantification kit (Waters, WAT054955). For proteome analysis, 20 μg of peptides were dried and resuspended in 0.1% formic acid for LC-MS/MS analysis. For phosphoproteome analysis, 800 μg of peptides were dried and subjected to phosphopeptide enrichment using the High-Select™ TiO2 Phosphopeptide Enrichment Kit (Thermo, A32993), followed by drying and resuspension in 0.1% formic acid for MS analysis.

Samples were analyzed by LC-MS/MS using a tandem nano elute system timsTOF Pro2 mass spectrometer (Bruker Daltonics), with a total of 250 ng of sample uploaded. The mass spectrometer operated in diaPASEF mode for DIA data acquisition, and the relevant methods are described in (https://doi.org/10.1016/j.cell.2024.12.024). For data analysis of proteomics, Spectronaut18 software was used for DIA data analysis with default parameters (BGS Factory Settings). The sequence database utilized was fas.fa (NCBI), and trypsin digestion was specified. Fixed modifications included carbamidomethylation (C) 57.02, and variable modifications included oxidation (M) 15.99 and phosphorylation of serine, threonine, and tyrosine (79.91). Protein identification criteria were set to a precursor threshold of 1.0% FDR and a protein threshold of 1.0% FDR. A decoy database was generated using the mutated strategy, creating a similar number of amino acid sequences shuffled (minimum 2 amino acids, maximum half of the total peptide length). Spectronaut performed automatic calibration and normalized data using a local normalization strategy, utilizing the average peak area of the top 3 peptides with FDR < 1.0% for protein group quantitation. Phosphorylation changes were quantified relative to peptide changes. All identified phosphopeptides are listed in Supplementary Table 1. Phosphopeptides from PSII and PSI subunits, identified in both replicates, with |log2 fold change| > 0.263 and an adjusted p-value < 0.05 were classified as significantly phospho-regulated peptides and listed in Supplementary Table 2.

Sample separation using lpBN-PAGE and lpCN-PAGE

LpBN-PAGE analysis was carried out according to the procedure described previously[40]. Thylakoid membranes equivalent to 50 μg of Chl were first pelleted at 8000 g for 5 min at 4 °C, then the supernatant was discarded. The pellet was resuspended in BTH buffer (25 mM Bis-Tris/HCl pH 7.0, 20% (w/v) glycerol, 10 mM sodium fluoride) followed centrifuged at 12000 g for 10 min at 4 °C, then resuspended in BTH buffer and recentrifuged as before. The pellet was solubilized in 95 μL BTH buffer contained either β-DM or digitonin with a final concentration of 1%. After solubilization for 10 min on ice (β-DM) or 5 min with continuous gentle agitation at room temperature, the insolubilized material was separated by centrifugation at 18000 g for 10 min at 4 °C. Finally, the supernatant contained 10 μL ACA buffer (100 mM Bis-Tris/HCl pH 7.0, 30% (w/v) glycerol, 5% G250, 0.5 M 6-aminocaproic acid) was used for the analysis of thylakoid membrane protein complexes by lp-BN-PAGE. The first-dimensional separation gel utilized in the experiment consisted of an acrylamide gradient of 3.5 – 12.5%. The ratio of bisacrylamide to total acrylamide in the gel was 3%. In the stacking gel, the total concentration of acrylamide was 3%, with a bisacrylamide-to-acrylamide ratio of 20%. Both gels were prepared using the gel buffer containing 0.5 M 6-aminocaproicacid and 50 mM BisTris/HCl pH 7.0. The anode buffer (50mM BisTris/HCl pH 7.0) and the cathode buffer (50mM Tricine, 15mM BisTris/HCl pH 7.0, 0.05%, 0.1% Coomassie Brilliant Blue) were used. For 2D separation of the individual protein subunits, the strips were incubated for 30 min in Laemmli buffer containing 10% (v/v) β-mercaptoethanol and subsequently runned by 15% SDS-PAGE. LpCN-PAGE was performed essentially as described previously[6]. The only difference with lp-BN-PAGE was that the cathode buffer (50mM Tricine, 15mM BisTris/HCl pH 7.0, 0.05% sodium deoxycholate) did not contain Coomassie Brilliant Blue or dodecyl maltoside because the former acted as a competitive quencher of chlorophyll fluorescence in LHCII, and

the latter deteriorated the megacomplex.

Gel fixation, staining, excision, and MALDI-TOF-TOF MS/MS analysis

Protein gel fixation, staining, excision, and MALDI-TOF-TOF MS/MS analysis were performed following a previously established method[58]. The gel shown in Supplementary Fig.5a was fixed overnight in a solution containing 50% (v/v) ethanol and 10% (v/v) orthophosphoric acid, washed with water for 1 hour, and subsequently stained with Colloidal Coomassie Blue G−250 (CCB) following the method described previously. Selected protein spots of interest were manually excised from the 2-DE gel and processed through de-staining, dehydration, reduction with dithiothreitol (DTT), alkylation with iodoacetamide, and digestion with gold-grade trypsin (Mass Grade, Promega). The digested samples were analyzed using a MALDI-TOF-TOF tandem mass spectrometer (ABI 4800 Proteomics Analyzer, Applied Biosystems, Framingham, MN). For mass spectrometry analysis, 0.4 μL of each sample was spotted onto a MALDI plate followed by the addition of 0.4 μL of matrix solution (0.5 M CHCA in 50% (v/v) acetonitrile (HPLC grade, Fisher) and 0.05% (v/v) trifluoroacetic acid (HPLC grade, Merck)). Mass spectra were acquired using 4000 Series Explorer Software v3.5 in batch processing mode for both MS and MS/MS. All MS survey scans were recorded in the mass range of m/z 800–4000 using the reflection positive-ion mode. MS peaks were detected with a minimum signal-to-noise ratio (S/N) ≥ 10 and a cluster area S/N threshold ≥ 40, without smoothing or raw spectrum filtering. Peptide precursor ions corresponding to contaminants such as keratin and trypsin autolytic products were excluded within a mass tolerance of 0.5 Da. For protein identification, the acquired MS/MS data were analyzed using Protein Pilot software (Applied Biosystems, Framingham, MN) and searched against the NCBI non-redundant protein sequence database (NCBI-nr) and the Swiss-Prot database. The search parameters included trypsin as the proteolytic enzyme, allowing for up to one missed cleavage; carbamidomethylation of cysteine was set as a fixed modification, while oxidation of methionine was considered a variable modification. Proteins with a Mowse score exceeding 60 (significant at a 95% confidence interval) were considered positively identified and are reported.

Modulated chlorophyll fluorescence techniques

The visible NPQ and *Fv/Fm* were measured using a modulated chlorophyll *a* fluorescence imager (CF imager, Technologica, UK). The system was equipped with a double-ring array of 96 LEDs providing actinic blue light, measuring light (~18 μmol photons m^{-2} s^{-1}), and saturating pulses (12,000 μmol photons m^{-2} s^{-1}, 600 ms duration) with a peak wavelength at 470 nm. A charge-coupled device (CCD) camera with a resolution of 640 × 480 pixels captured fluorescence images, which were visualized using a false-color scale (0 −1). For each measurement, plants were dark-acclimated for >30 min before measurement. The minimal fluorescence yield (*Fo*) was recorded under measuring light, and the maximal fluorescence yield (*Fm*) was measured immediately after applying a saturating pulse. *Fv/Fm* was calculated as $(Fm - Fo)/Fm$. To assess NPQ, leaves were exposed to actinic light (1,066 μmol photons m^{-2} s^{-1}) for 10 min to induce steady-state photosynthesis. Subsequently, leaves were dark-adapted for 5 min, and NPQ was calculated as $(Fm - Fm')/Fm'$, where Fm' is the maximal fluorescence yield under actinic light.

The steady-state light response curves was measured with the Dual PAM100 (Walz, Effeltrich, Germany). Fully dark-adapted leaves (30 min) were exposed to a series of actinic light intensities ranging from 0 to 1805 μmol photons m^{-2} sec^{-1}. Each light intensity was maintained for 2 min to ensure attainment of steady-state photosynthetic conditions, during which chlorophyll fluorescence parameters were recorded. Fluorescence parameters and coefficients were defined according to Rohácek[59]. The following yield values were calculated as described by Hendrickson et al. (2004)[60]: The yields of PSII

photochemistry (Y(PSII) = (*Fm′-F*)/*Fm′*), regulated thermal dissipation (Y(NPQ) = *F*/*Fm ′- F*/*Fm*) and constitutive energy loss (Y(NO) = *F*/*Fm*, which includes non-regulated thermal dissipation in PSII and fluorescence emission) were calculated as described in previous studies[27].

The state transition were monitored with the Dual PAM100 based on an experiment procedure described previously[27]. Dark-adapted (12 h) leaves were first exposed to HL (800 μmol photons m^{-2} s^{-1}) for 10 min, followed by far-red light application for 10 min in the background of HL. The experimental sequence was repeated. During the experiment, a saturated pulse was used every minute to obtain the *Fm′/Fm*, which can reflect the change of PSII fluorescence. If P-CP24 was involved in the state transition in HL, the *Fm′/Fm* should increase in FR light duo to a transition to state 1 in the background of HL. It can also be reverted by turn off FR light in the background of white HL.

For NPQ measurements on dark-adapted leaves, the Dual PAM−100 system was used. NPQ induction of leaves from dark-adapted 30 min plants was measured by exposed them to GL (50 μmol photons m^{-2} s^{-1}) or HL (800 μmol photons m^{-2} s^{-1}) for 10 min. Subsequently, NPQ relaxation was followed during a 20 min in darkness. The NPQ components were resolved in semi-logarithmic plots based on their $t_{1/2}$ values as described in previous studies[27,61]. In the time scale used for relaxation experiments, NPQ relaxed biphasically. The residual NPQ fraction after 20 min approximated qI, which is almost irreversible over such an interval (Lichtenthaler et al., 2005).

For NPQ measurements on functional chloroplasts, isolated chloroplasts (40 mg chlorophyll/mL) were suspended in buffer containing 10 mM methylviologen, 0.5 mM ATP, and 15 mM Asc. Chloroplast samples were divided into three groups: (1) wild-type with ATP and CP24 phosphorylation inhibitor k252a (WT + ATP + k252a), (2) wild-type with ATP only (WT + ATP), and (3) wild-type control without k252a and ATP (WT). Each 1.5 mL aliquot was loaded into a 3 mL quartz cuvette with a magnetic rotor to prevent sedimentation during measurements. NPQ was induced by 800 μmol photons m^{-2} s^{-1} illumination for 16 min, followed by 10 min of dark relaxation to monitor quenching recovery using the Dual PAM100.

For *Fv/Fm* measurements on functional chloroplasts, the chloroplasts were first exposed to HL of 1000 μmol photons m^{-2} s^{-1} followed by 30 min dark-adaption, and then *Fv/Fm* were measured using the Dual-PAM−100 system.

Singlet oxygen production analysis

Singlet oxygen production in functional chloroplasts was measured as described previously[51]. Briefly, the functional chloroplasts at 80 μg/ml concentration in a solution containing 0.03% α-DM, 20 mM Hepes, pH 7.5, 2 μM Single Oxygen Sensor Green™[62], 20 mM ATP and with or without k252a were illuminated at 1000 μmol photons m^{-2} s^{-1} for different times. The increase of the concentration of singlet oxygen in solution was detected by measuring the Sensor Green specific fluorescence at 530 nm, with a 480 nm excitation.

Purification of recombinant PBCP (rPBCP) and dephosphorylation assays of P-CP24

The cDNA of *B. incana* was used as the template for PCR amplification, with primers designed based on the 20-bp upstream and downstream flanking sequences of the AtPBCP cDNA. Chloroplast transition peptide was determined using ChloroP method. cDNA sequences of the predicted mature PBCP proteins were cloned into pET28a (Invitrogen) to include a C-terminal 6×His tag and expressed in Escherchia coli strain BL21. IPTG was added to induce expression of the PBCP protein at 16 °C for 20 h. Following cell lysis and centrifugation at 8000 g, the supernatant containing recombinant PBCP was loaded onto Ni-nitrilotriacetic acid (Ni-NTA) resin (Qiagen). The Ni-NTA was washed with PBS buffer with 30 mM imidazole, and rPBCP was eluted with PBS buffer containing 300 mM imidazole.

Recombinant PBCP eluted at the expected size of 30 kD was concentrated to stocks of 1 mg/ml. Subsequently, 1 μg rPBCP was incubated together with thylakoid membranes corresponding to 1 μg total chlorophylls in the dephosphorylation buffer contained 25 mM Tricine-NaOH (pH 7.8), 100 mM sorbitol, 10 mM KCl, 5 mM $MgCl_2$, and 10 mM DTT as described previously[24].

Identification and quantification of pigments by HPLC

Pigments were extracted from chloroplast samples[63] and analyzed by HPLC as described previously[64] with slight modifications. HPLC was performed with a C−18 reversed-phase column (4.6 mm×250 mm, 5 μm particle size, Grace, USA) in a Waters e2695 separation module equipped with a Waters 2998 photodiode array detector. The pigments were eluted at a flow rate of 1 ml min^{-1} using solvent A (acetonitrile: methanol, 75: 25) for the first 9 min, followed by a 3 min linear gradient with solvent B (methanol: ethylacetate, 70: 30), which continued isocratically until the end of the 27 min separation. The column was re-equilibrated in solvent A at a flow rate of 1 ml min^{-1} for 10 min prior to the next injection. Pigments were detected by their absorbance at 440 nm. The standard samples of Chl *a*, Chl *b*, zeaxanthine and lutein used were purchased from Sigma-Aldrich. The addition of Asc, a cofactor of violaxanthin de-epoxidase, is essential for the detection of zeaxanthin.

Steady state fluorescence and time-resolved fluorescence analysis

Low-temperature (77 K) spectra were recorded on thylakoid membranes (5 μg total Chl mL^{-1}), by using a F-700 fluorescence spectrofluorimeter (Hitachi, Ltd, Japan). For the emission spectra, excitation was defined at 436 nm with a 5 nm bandwidth, with emission being measured between 600 and 800 nm. Each spectrum was taken three times, and normalised at 0 and 1. Time-resolved fluorescence spectra were measured with time-correlated single-photon counting system at 77 K as described previously[65]. Excitation wavelength was 480 nm. The time interval for data acquisition was set 26 ps/channel. Spectral data were measured with a 2-nm interval. Fluorescence rise and decay curves were analyzed by global analysis[66] to obtain fluorescence decay-associated spectra (FDAS).

Room-temperatrure fluorescence decay analysis

Time-resolved fluorescence decays at room temperature (23°C) were acquired using time-correlated single-photon counting on a FluoroCube (HORIBA Jobin-Yvon), as previously described[32]. The complex was excised from the lpCN-PAGE and placed on the FluoroCube. Chlorophylls were excited at 463 nm with a picosecond pulse diode laser (DD-470L; HORIBA Jobin Yvon) operating at a 10-MHz repetition rate (1.64 pJ per pulse). Emission was detected at 695 nm through a monochromatic detector with a bandwidth of 8 nm.

Competing interests

The authors declare no competing interests

References

1 Dogra, V., Li, M., Singh, S., Li, M. & Kim, C. Oxidative post-translational modification of EXECUTER1 is required for singlet oxygen sensing in plastids. *Nat. Commun.* **10**, 2834 (2019).

2 Bethmann, S., Melzer, M., Schwarz, N. & Jahns, P. The zeaxanthin epoxidase is degraded along with the D1 protein during photoinhibition of photosystem II. *Plant Direct* **3**, 1−13 (2019).

3 Erickson, E., Wakao, S. & Niyogi, K. K. Light stress and photoprotection in *Chlamydomonas reinhardtii*. *Plant J.* **82**, 449-465 (2015).

4 Pinnola, A. & Bassi, R. Molecular mechanisms involved in plant photoprotection. *Biochem. Soc. Trans.* **46**, 467-482 (2018).

5 Chmeliov, J. *et al.* Aggregation-Related Nonphotochemical Quenching in the Photosynthetic Membrane. *J. Phys. Chem. Lett.* **10**, 7340-7346 (2019).
6 Yokono, M., Takabayashi, A., Akimoto, S. & Tanaka, A. A megacomplex composed of both photosystem reaction centres in higher plants. *Nat. Commun.* **6**, (2015).
7 Zhu, X. G., Long, S. P. & Ort, D. R. What is the maximum efficiency with which photosynthesis can convert solar energy into biomass? *Curr. Opin. Biotechnol.* **19**, 153−159 (2008).
8 Kromdijk, J. *et al.* Improving photosynthesis and crop productivity by accelerating recovery from photoprotection. *Science* **354**, 857-861 (2016).
9 De Souza, A. P. *et al.* Soybean photosynthesis and crop yield are improved by accelerating recovery from photoprotection. *Science* **377**, 851-854 (2022).
10 Bellafiore, S., Barneche, F., Peltier, G. & Rochaix, J. D. State transitions and light adaptation require chloroplast thylakoid protein kinase STN7. *Nature* **433**, 892-895 (2005).
11 Crepin, A. & Caffarri, S. The specific localizations of phosphorylated Lhcb1 and Lhcb2 isoforms reveal the role of Lhcb2 in the formation of the PSI-LHCII supercomplex in *Arabidopsis* during state transitions. *Biochimica et Biophysica Acta (BBA) - Bioenergetics* **1847**, 1539−1548 (2015).
12 Pan, X. W. *et al.* Structure of the maize photosystem I supercomplex with light-harvesting complexes I and II. *Science* **360**, 1109−1112 (2018).
13 Rintamäki, E., Martinsuo, P., Pursiheimo, S. & Aro, E. M. Cooperative regulation of light-harvesting complex II phosphorylation via the plastoquinol and ferredoxin-thioredoxin system in chloroplasts. *Proceedings of the National Academy of Sciences of the United States of America* **97**, 11644−11649 (2000).
14 Shapiguzov, A. *et al.* The PPH1 phosphatase is specifically involved in LHCII dephosphorylation and state transitions in *Arabidopsis*. *Proceedings of the National Academy of Sciences of the United States of America* **107**, 4782-4787 (2010).
15 Pribil, M., Pesaresi, P., Hertle, A., Barbato, R. & Leister, D. Role of plastid protein phosphatase TAP38 in LHCII dephosphorylation and thylakoid electron flow. *PLoS Biol.* **8**, e1000288 (2010).
16 Li, X. P. *et al.* Regulation of photosynthetic light harvesting involves intrathylakoid lumen pH sensing by the PsbS protein. *J. Biol. Chem.* **279**, 22866−22874 (2004).
17 Chiariello, M. G., Gru, F., Zarmiento-Garcia, R. & Marrink, S. J. pH-Dependent Conformational Switch Impacts Stability of the PsbS Dimer. *J. Phys. Chem. Lett.* **14**, 905-911 (2023).
18 Correa-Galvis, V., Poschmann, G., Melzer, M., Stuhler, K. & Jahns, P. PsbS interactions involved in the activation of energy dissipation in *Arabidopsis*. *Nat. Plants* **2**, 1-8 (2016).
19 Luca Dall'Osto, Stefano Cazzaniga & Mauro Bressan, D. P., Karel Židek, Krishna K. Niyogi, Graham R. Fleming, Donatas Zigmantas and Roberto Bassi. Two mechanisms for dissipation of excess light in monomeric and trimeric light-harvesting complexes. *Nat. Plants* **3**, 1-9 (2017).
20 Chen, L., Rodriguez Heredia, M., Hanke, G. T. & Ruban, A. V. Distinct features of PsbS essential for mediating plant photoprotection. *Plant Commun.*, 101179 (2024).
21 Fristedt, R. *et al.* Phosphorylation of photosystem II controls functional macroscopic folding of photosynthetic membranes in *Arabidopsis*. *The Plant Cell* **21**, 3950-3964 (2009).
22 Baena González, E., Barbato, R. & Aro, E. M. Role of phosphorylation in the repair cycle and oligomeric structure of photosystem II. *Planta* **208**, 196−204 (1999).
23 Betterle, N. *et al.* The STN8 kinase-PBCP phosphatase system is responsible for high-light-

induced reversible phosphorylation of the PSII inner antenna subunit CP29 in rice. *Plant J.* **89**, 681-691 (2017).

24 Samol, I. *et al.* Identification of a photosystem II phosphatase involved in light acclimation in *Arabidopsis*. *The Plant Cell* **24**, 2596−2609 (2012).

25 Krishna, N. *et al.* Towards a critical understanding of the photosystem II repair mechanism and its regulation during stress conditions. *FEBS Lett.* **587**, 3372-3381 (2013).

26 Betterle, N., Ballottari, M., Baginsky, S. & Bassi, R. High light-dependent phosphorylation of Photosystem II inner antenna CP29 in monocots Is STN7 independent and enhances nonphotochemical quenching. *Plant Physiol.* **167**, 457-U714 (2015).

27 Ferroni, L. *et al.* Light-dependent reversible phosphorylation of the minor photosystem II antenna Lhcb6 (CP24) occurs in lycophytes. *Plant J.* **77**, 893-905 (2014).

28 Fristedt, R. & Vener, A. V. High light induced disassembly of photosystem II supercomplexes in *Arabidopsis* requires STN7-dependent phosphorylation of CP29. *PLoS One* **6**, e24565 (2011).

29 Reiland, S. *et al.* Large-scale *Arabidopsis* phosphoproteome profiling reveals novel chloroplast kinase substrates and phosphorylation networks. *Plant Physiol.* **150**, 889-903 (2009).

30 Roitinger, E. *et al.* Quantitative phosphoproteomics of the Ataxia Telangiectasia-Mutated (ATM) and Ataxia Telangiectasia-Mutated and Rad3-related (ATR) dependent DNA damage response in *Arabidopsis thaliana*. *Mol. Cell. Proteomics* **14**, 556-571 (2015).

31 Bag, P. *et al.* Direct energy transfer from photosystem II to photosystem I confers winter sustainability in Scots Pine. *Nat. Commun.* **12**, 1662 (2021).

32 Kotaro, K. *et al.* LHCSR1-dependent fluorescence quenching is mediated by excitation energy transfer from LHCII to photosystem I in *Chlamydomonas reinhardtii*. *Proceedings of the National Academy of Sciences of the United States of America* **115**, 3722–3727 (2018).

33 You, X. *et al.* In situ structure of the red algal phycobilisome–PSII–PSI–LHC megacomplex. *Nature* **616**, 199−206 (2023).

34 Wu, L. S. *et al.* Photosynthetic inner antenna CP47 plays important roles in ephemeral plants in adapting to high light stress. *J. Plant Physiol.* **251**, 153189 (2020).

35 Su, X. D. *et al.* Structure and assembly mechanism of plant $C_2S_2M_2$-type PSII-LHCII supercomplex. *Science* **357**, 815–820 (2017).

36 Wilson, S. & Ruban, A. V. Enhanced NPQ affects long-term acclimation in the spring ephemeral *Berteroa incana*. *Biochimica Et Biophysica Acta-Bioenergetics* **1861**, 148014 (2020).

37 Tu, W. *et al.* Diminished photoinhibition is involved in high photosynthetic capacities in spring ephemeral *Berteroa incana* under strong light conditions. *J. Plant Physiol.* **169**, 1463−1470 (2012).

38 Gerotto, C. *et al.* Thylakoid protein phosphorylation dynamics in a moss mutant lacking serine/threonine protein kinase STN8. *Plant Physiol.* **180**, 1582−1597 (2019).

39 Roberto Barbato, E. B., Ildiko` Szabo`, Francesca Dalla Vecchia, and Giorgio M. Giacometti. Ultraviolet B exposure of whole leaves of barley affects structure and functional organization of Photosystem II. *J. Biol. Chem.* **275**, 10976–10982 (2000).

40 Jarvi, S., Suorsa, M., Paakkarinen, V. & Aro, E. M. Optimized native gel systems for separation of thylakoid protein complexes: novel super- and mega-complexes. *Biochem. J.* **439**, 207−214 (2011).

41 Ferroni, L., Suorsa, M., Aro, E. M., Baldisserotto, C. & Pancaldi, S. Light acclimation in the lycophyte *Selaginella martensii* depends on changes in the amount of photosystems and on the

flexibility of the light-harvesting complex II antenna association with both photosystems. *New Phytol.* **211**, 554-568 (2016).

42 Chen, Y. E. *et al.* Phosphorylation of photosynthetic antenna protein CP29 and photosystem II structure changes in monocotyledonous plants under environmental stresses. *Biochemistry* **48**, 9757-9763 (2009).

43 Kargul, J. *et al.* Light-harvesting complex II protein CP29 binds to photosystem I of *Chlamydomonas reinhardtii* under State 2 conditions. *FEBS J.* **272**, 4797-4806 (2005).

44 Croce, R. & van Amerongen, H. Light harvesting in oxygenic photosynthesis: Structural biology meets spectroscopy. *Science* **369**, eaay2058 (2020).

45 Bonardi, V. *et al.* Photosystem II core phosphorylation and photosynthetic acclimation require two different protein kinases. *Nature* **437**, 1179−1182 (2005).

46 Kato, Y. & Sakamoto, W. Phosphorylation of photosystem II core proteins prevents undesirable cleavage of D1 and contributes to the fine-tuned repair of photosystem II. *Plant J.* **79**, 312-321 (2014).

47 Pesaresi, P., Pribil, M., Wunder, T. & Leister, D. Dynamics of reversible protein phosphorylation in thylakoids of flowering plants: the roles of STN7, STN8 and TAP38. *Biochimica et Biophysica Acta (BBA) - Bioenergetics* **1807**, 887-896 (2011).

48 Roitinger, E. *et al.* Quantitative Phosphoproteomics of the Ataxia Telangiectasia-Mutated (ATM) and Ataxia Telangiectasia-Mutated and Rad3-related (ATR) Dependent DNA Damage Response in. *Mol. Cell. Proteomics* **14**, 556-571 (2015).

49 Saccon, F., Giovagnetti, V., Shukla, M. K. & Ruban, A. V. Rapid regulation of photosynthetic light harvesting in the absence of minor antenna and reaction centre complexes. *J. Exp. Bot.* **71**, 3626-3637 (2020).

50 Ruban, A. V. Unveiling the atomic-scale transition between light harvesting and photoprotective states in plant photosynthesis. *Sci. China Chem.* **67**, 1375−1377 (2024).

51 Betterle, N., Ballottari, M., Hienerwadel, R., Dall'Osto, L. & Bassi, R. Dynamics of zeaxanthin binding to the photosystem II monomeric antenna protein Lhcb6 (CP24) and modulation of its photoprotection properties. *Arch. Biochem. Biophys.* **504**, 67-77 (2010).

52 Paolo, P., Dorianna, S., Elisabetta, G. & Bassi, R. A single point mutation (E166Q) preven dicyclohexylcarbodumide binding to the photosystem II subunit CP29 *FEBS Lett.* **402**, 151−156 (1997).

53 Cignoni, E. *et al.* A different perspective for nonphotochemical quenching in plant antenna complexes. *Nat. Commun.* **12**, 7152 (2021).

54 Ruan, M. *et al.* Cryo-EM structures of LHCII in photo-active and photo-protecting states reveal allosteric regulation of light harvesting and excess energy dissipation. *Nat. Plants* **9**, 1547−1557 (2023).

55 Steffen, G. *et al.* Specific thylakoid protein phosphorylations are prerequisites for overwintering of Norway pruce (*Picea abies*) photosynthesis. *Proceedings of the National Academy of Sciences of the United States of America* **117**, 17499−17509 (2020).

56 Zhang, L. X., Paakkarinen, V., van Wijk, K. J. & Aro, E. M. Co-translational assembly of the D1 protein into photosystem II. *J. Biol. Chem.* **274**, 16062−16067 (1999).

57 Casazza, A. P., Tarantino, D. & Soave, C. Preparation and functional characterization of thylakoids from *Arabidopsis thaliana*. *Photosynth. Res.* **68**, 175−180 (2001).

58 Zhang, J. *et al.* Proteomic analysis and candidate allergenic proteins in Populus deltoides CL.

"2KEN8" mature pollen. *Front. Plant Sci.* **6** (2015).

59 Rohácek, K. Chlorophyll fluorescence parameters: the definitions, photosynthetic meaning, and mutual relationships. *Photosynthetica* **40**, 13−29 (2002).

60 Hendrickson, L., Furbank, R. T. & Chow, W. S. A simple alternative approach to assessing the fate of absorbed light energy using chlorophyll fluorescence. *Photosynth. Res.* **82**, 73-81 (2004).

61 Horton, P. & Hague, a. A. Studies on the induction of chlorophyll fluorescence in isolated barley protoplasts. IV. Resolution of n0n-photochemical quenching. *Biochimica et Biophysica Acta (BBA) - Bioenergetics* **932**, 107−115 (1988).

62 Flors, C. *et al.* Imaging the production of singlet oxygen using a new fluorescent sensor, Singlet Oxygen Sensor Green®. *J. Exp. Bot.* **57**, 1725−1734 (2006).

63 Paulsen, H., Rumler, U. & Rudiger, W. Reconstitution of pigment-containing complexes from light-harvesting chlorophyll-a/B-binding protein overexpressed in Escherichia-Coli. *Planta* **181**, 204−211 (1990).

64 Qin, X. C., Michihiro, S., Tingyun, K. & Shen, J. R. Structural basis for energy transfer pathways in the plant PSI-LHCI supercomplex. *Science* **348**, 989-995 (2015).

65 Yokono, M., Murakami, A. & Akimoto, S. Excitation energy transfer between photosystem II and photosystem I in red algae: larger amounts of phycobilisome enhance spillover. *Biochimica et Biophysica Acta (BBA) - Bioenergetics* **1807**, 847-853 (2011).

66 Ivo H.M. van Stokkum, Delmar S. Larsen & Rienk van Grondelle. Global and target analysis of time-resolved spectra. *Biochimica et Biophysica Acta (BBA) - Bioenergetics* **1657**, 82−104 (2004).

Figure legends

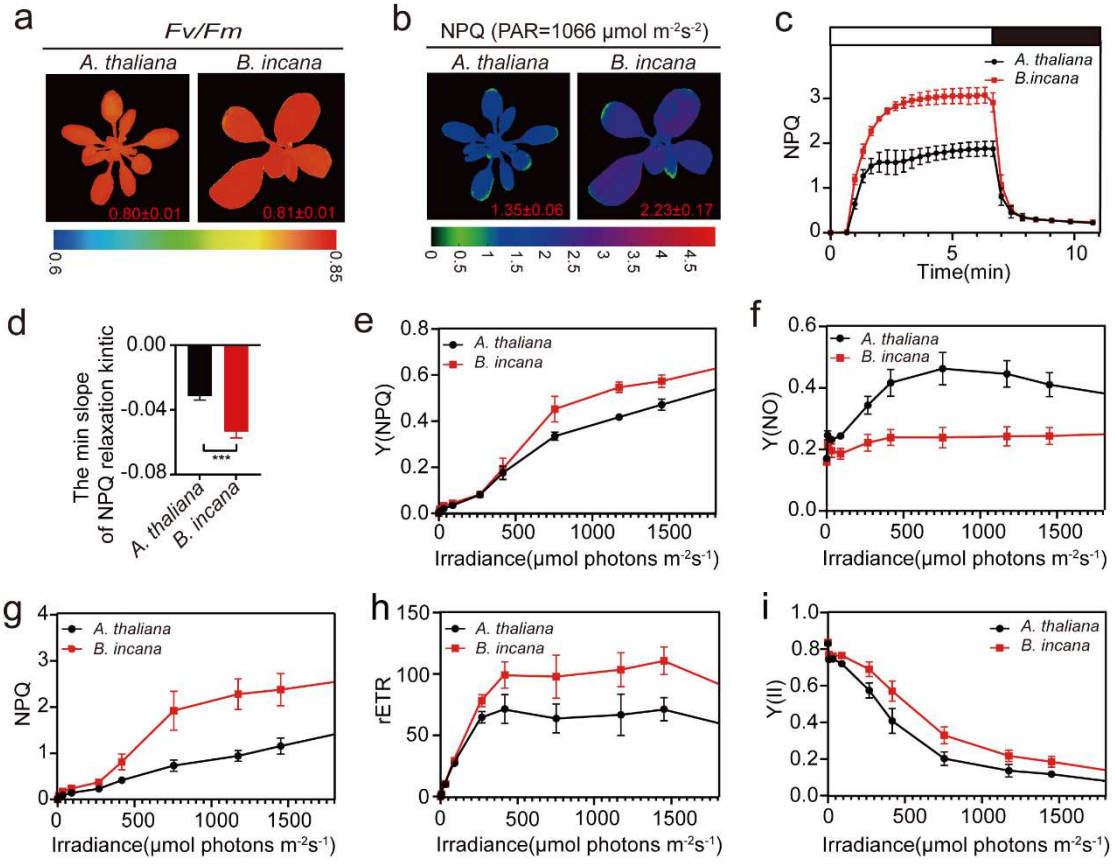

Figure 1: *B. incana* maintains superior photoprotection and PSII stability relative to *A. thaliana* under HL conditions via enhanced NPQ

a The maximal quantum yield of PSII in *B. incana* and *A. thaliana*, presented as the *Fv/Fm* ratio following dark acclimation, visualized as false-color images. **b** Comparative visualization of NPQ phenotypes under 1066 μmol photons m^{-2} s^{-1} in *B. incana* and *A. thaliana* using chlorophyll fluorescence imaging. Representative images show NPQ values. Data are means ± standard deviation (SD) from at least three independent biological replicates. **c** Dual-PAM characterization of NPQ kinetics in *B. incana* and *A. thaliana*. NPQ kinetics were monitored over a 360 s HL illumination period (1066 μmol photons m^{-2} s^{-1}), followed by a 240 s dark relaxation phase. White and black bars in the panel denote the illumination and dark periods, respectively. Data are means ± SD from at least five independent biological replicates. **d** Minimum slope of NPQ relaxation immediately after lights-off derived from the data in panel (**c**) **e – i** Light-response curves of key photosynthetic parameters: measured after 30 min dark adaptation, at increasing light intensities (2 min per measurement). **e** Quantum yield of regulated thermal dissipation (Y(NPQ)). **f** Quantum yield of non-regulated thermal dissipation (Y(NO)). **g** Non-photochemical quenching (NPQ). **h** Relative linear electron transport rate (rETR). **i** Quantum yield of PSII photochemistry (Y(II)). All symbols and error bars represent the mean ± SD calculated from at least three independent biological replicates.

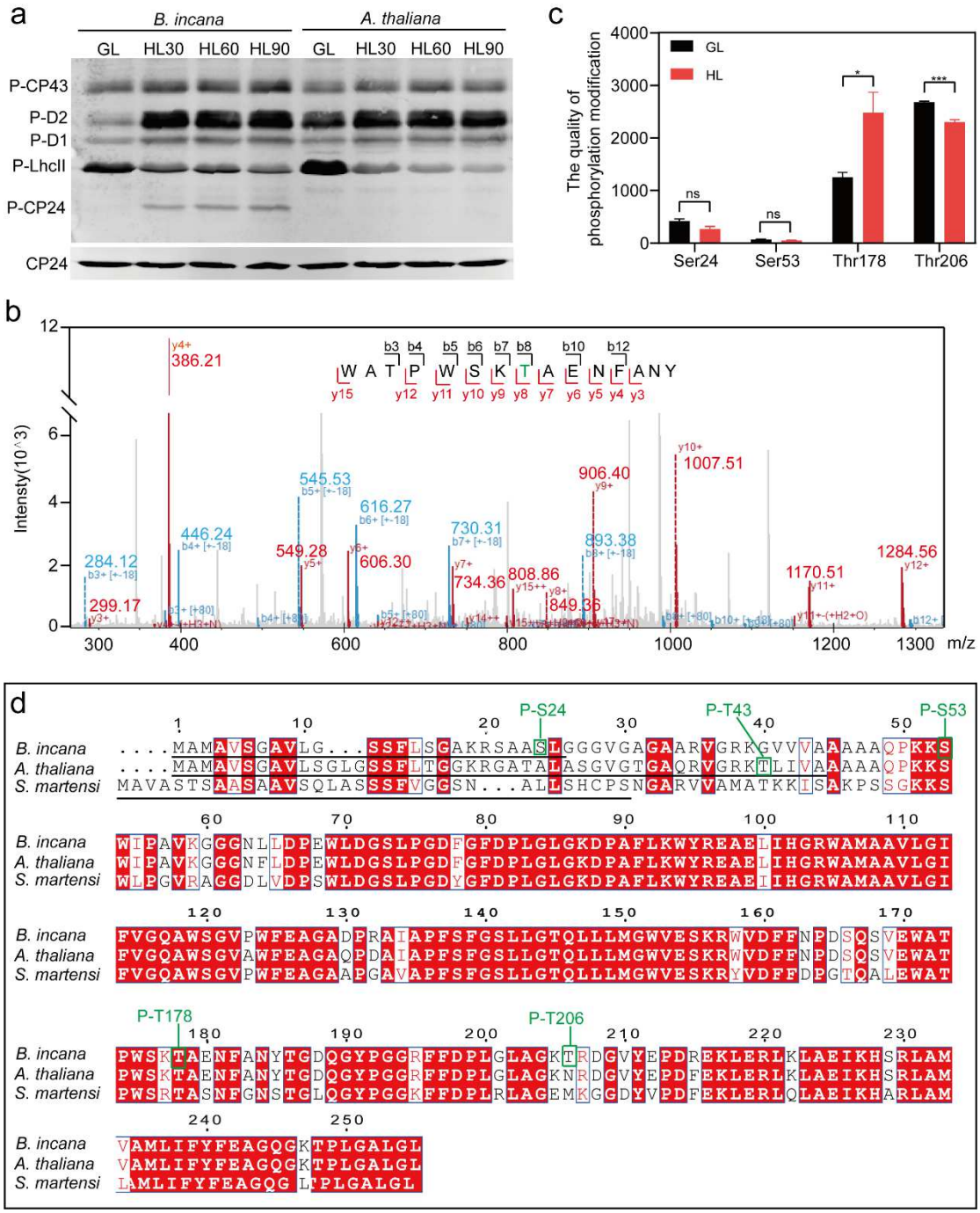

Figure 2: HL induces enhancement of CP24 phosphorylation

a Comparison of PSII phosphoproteins between *B. incana* and *A. thaliana*. Plants grown under growth light (GL,100 μmol photons m^{-2} s^{-1}) were exposed to high light (HL, 1,000 μmol photons m^{-2} s^{-1} for 30, 60 and 90 min), respectively. All lanes were loaded with 2 μg chlorophyll (Chl). **b** Mass spectrometric identification of the phosphopepide of CP24 contained P-Thr178. The peptide was dissociated using higher energy colision-induced disociation in mass spectrometer, which can break peptide bonds and yield a series of b and y ions. **c** Quantification of phosphopeptide of CP24 protein. Data are presented as mean ± SD (n=2). The abundance of phosphorylated CP24 peptides under HL treatment was compared with that under GL conditions using unpaired two-tailed t-tests. Statistical significance was defined as follows: *$p < 0.05$; **$p < 0.01$; ns, not significant. **d** Multiple sequence alignment of CP24 from *B.*

incana, *A. thaliana* and *S. martensi*. Chloroplast transport peptides determined using ChloroP1.1 online software are marked with black lines below the amino acid sequence. The phosphorylated site were labeled with a green box.

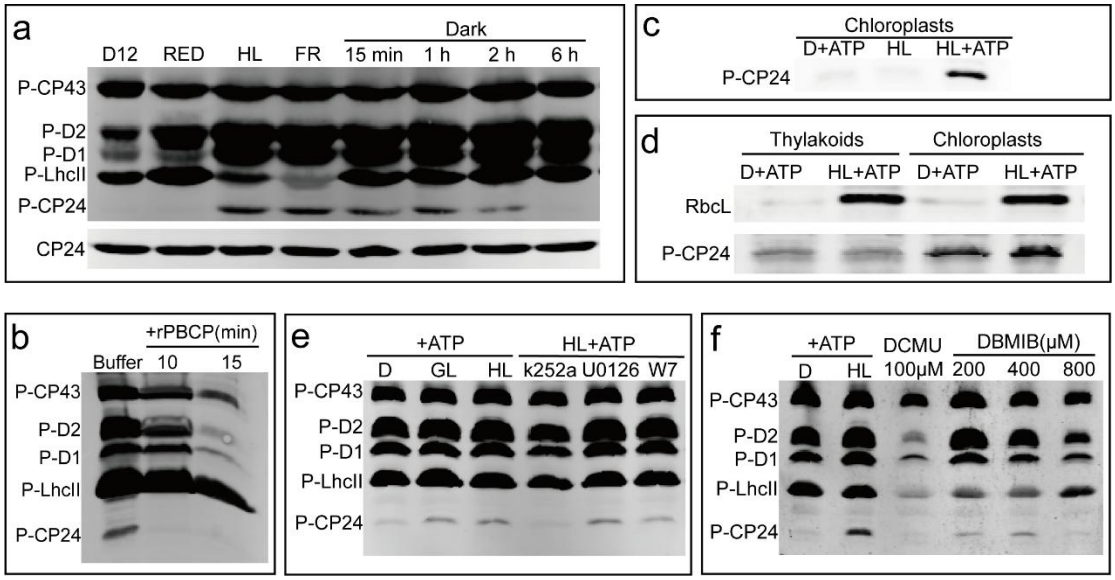

Figure 3: Characteristics of kinase and phosphatase regulating CP24 phosphorylation

a In vivo reversibility phosphorylation of CP24 in *B. incana*. Plants were dark adapted for 12 hours (D12) and then subjected to PSII light (red light, RED) at an intensity of 30 μmol photons m^{-2} s^{-1}) or high light (HL, 1000 μmol photons m^{-2} s^{-1}) for 2 hours. For recovery assays, HL-treated plants were transferred to darkness at defined intervals (15min – 6h), or exposed to PSI light (Far-red light (FR) at an intensity of 6 μmol photons m^{-2} s^{-1}) for 15min to monitor phosphorylation levels. **b** Recombinant PBCP (rPBCP) of *B. incana* can dephosphorylate P-CP24. Thylakoid membranes were illuminated for 30 min with white light (1000 μmol photons m^{-2} s^{-1}) in the presence of ATP and then incubated for 10 or 15 min in the dark in the presence of 5 μg rPBCP in the dephosphorylation buffer. As a control, samples were resuspended in the dephosphorylation buffer and then incubated in the dark for 15 minutes. **c** In vitro phosphorylation of CP24 in isolated functional chloroplasts. Chloroplasts were exposed to HL (1000 μmol photons m^{-2} s^{-1}) for 30 min in the presence (HL + ATP) or absence of ATP (HL) or were adapted in the dark for 30 min in the presence of ATP (D + ATP). **d** Localization of CP24 kinase was detected by inducing CP24 phosphorylation in functional chloroplasts or thylakoids, illuminated with white light (1000 μmol photons m^{-2} s^{-1}) for 30 min in the presence of ATP or were adapted in the dark for 30 min in the presence of ATP (D + ATP). **e** Effect of kinase inhibitors on CP24 phosphorylation in functional chloroplasts. Inhibitors used were k252a, W7 and U0126. The functional chloroplasts were illuminated with white light (1000 μmol photons m^{-2} s^{-1}) for 30 min in the presence of these chemicals. **f** Effect of electron transfer inhibitors on CP24 phosphorylation in functional chloroplasts. The functional chloroplasts were illuminated with white light (1000 μmol photons m^{-2} s^{-1}) for 30 min in the presence of DCMU or DBMIB. Immunodetection was performed using anti-P-Thr, anti-CP24 and anti-Rubisco (RbcL) antibody, respectively. All lanes were loaded with 3 μg Chl.

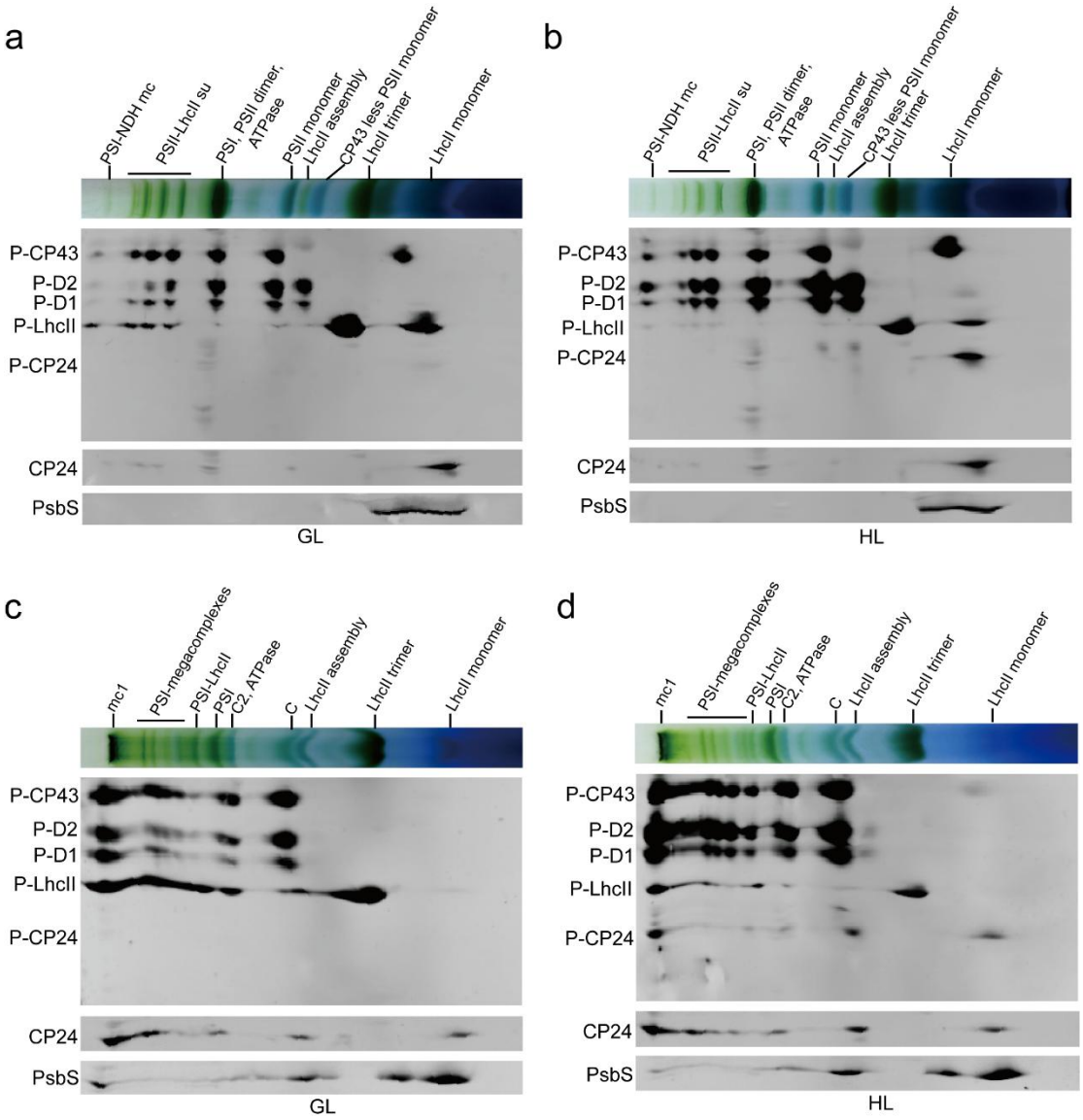

Figure 4: Native localization of phosphorylated CP24 in *B. incana*

a Thylakoid membranes isolated from *B. incana* grown under GL (100 µmol photons m^{-2} s^{-1}) were solubilized with β-dodecyl maltoside (β-DM, final concentration of 1% (w/v)) and subsequently separated by lp-BN/SDS-PAGE. **b** Thylakoid membranes isolated from *B. incana* exposed to HL (1000 µmol photons m^{-2} s^{-1}) for 1 h were solubilized with β-dodecyl maltoside (β-DM, final concentration of 1% (w/v)) and subsequently separated by lp-BN/SDS-PAGE. **c** Thylakoid membranes isolated from *B. incana* grown under GL (100 µmol photons m^{-2} s^{-1}) were solubilized with digitonin (dig, final concentration of 1% (w/v)) and subsequently separated by lp-BN/SDS-PAGE. **d** Thylakoid membranes isolated from *B. incana* exposed to HL (1000 µmol photons m^{-2} s^{-1}) for 1 h were solubilized with digitonin (dig, final concentration of 1% (w/v)) and subsequently separated by lp-BN/SDS-PAGE. For lp-BN/SDS-PAGE, 10 µg of Chl was loaded per lane. Immunodetection was performed using anti-P-Thr, anti-CP24, and anti-PsbS antibodies, respectively.

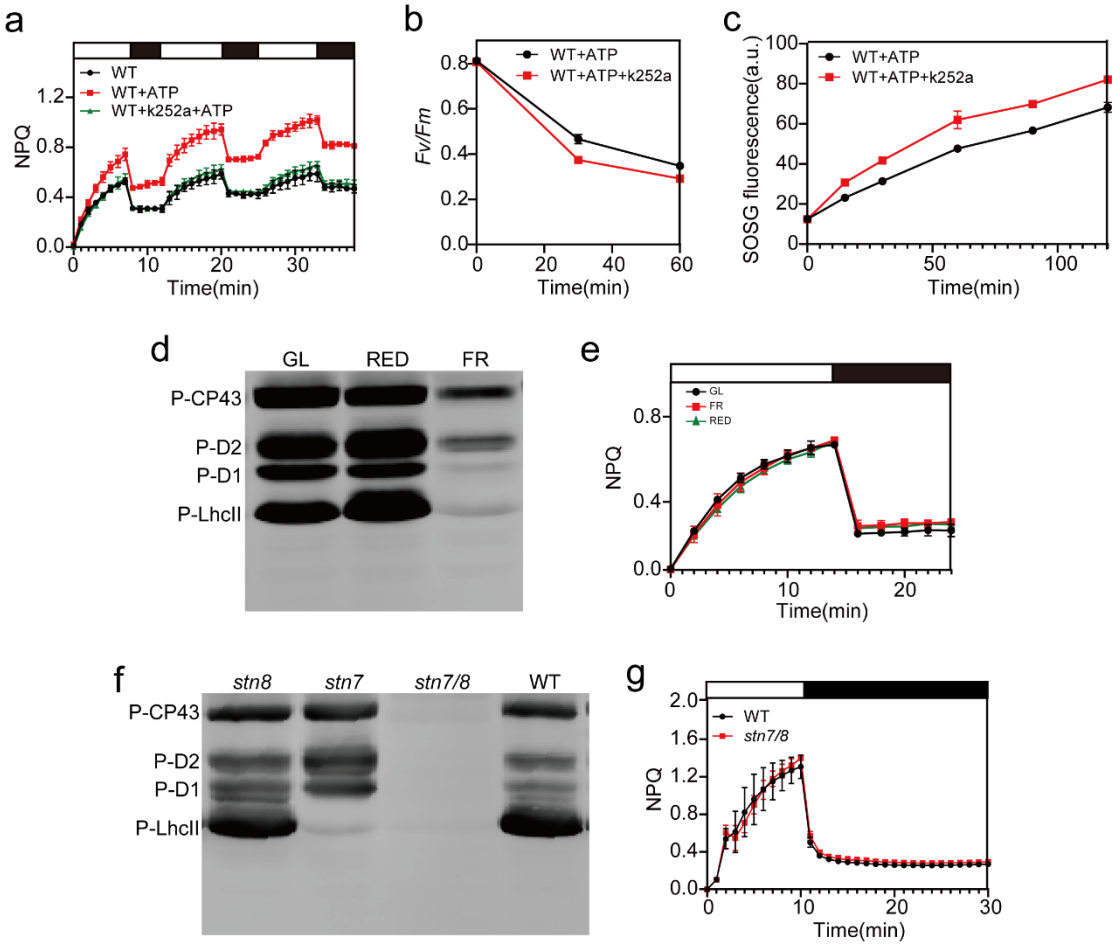

Figure 5: Effect of CP24 phosphorylation on photoprotection in functional chloroplasts

a NPQ Kinetics in *B. incana* chloroplasts. NPQ kinetics were monitored during three consecutive illumination cycles, each consisting of 15 min exposure to actinic light (1000 µmol photons m^{-2} s^{-1}) followed by a 10 min dark recovery period. **b** Maximal quantum yields of PSII (*Fv/Fm*) in *B. incana* Chloroplasts.The *Fv/Fm* was measured in chloroplasts isolated from *B. incana* after exposure to actinic light (1000 µmol photons m^{-2} s^{-1}) for 30 min or 60 min, in the presence or absence of the protein kinase inhibitor k252a. **c** Singlet oxygen production ($^1O_2$) in chloroplasts. The generation of $^1O_2$ in isolated chloroplasts was quantified at multiple time points using the fluorescent probe Singlet Oxygen Sensor Green (SOSG). Experiments were performed under control conditions (absence of k252a) and in the presence of the protein kinase inhibitor k252a. **d** Immunodetection of thylakoid phosphoproteins in *B. incana* under different light conditions. Thylakoid membrane phosphoproteins were isolated from *B. incana* plants grown under growth light (100 µmol photons m^{-2} s^{-1}) and exposed to either: PSII light (RED) for 2 hours, or PSI light (FR) for 4 hours. Immunodetection was performed to analyze light-specific phosphorylation patterns. **e** NPQ kinetics in chloroplasts isolated from leaves exposed to three light qualities as described in (**d**) and activated by actinic light (1000 µmol photons m^{-2} s^{-1}). **f** Immunodetection of thylakoid phosphoproteins isolated from *A. thaliana* wild-type (WT), *stn7*, *stn8* and *stn7/8* mutant. Samples were analyzed using an anti-P-Thr antibody. **g** NPQ kinetics of *A. thaliana* WT and *stn7/8* mutant with actinic light of 1000 µmol photons m^{-2} s^{-1}. For immunodetection experiments, all lanes were loaded with 3 µg Chl. Symbols and error bars show mean ± SD from at least three biological replicates.

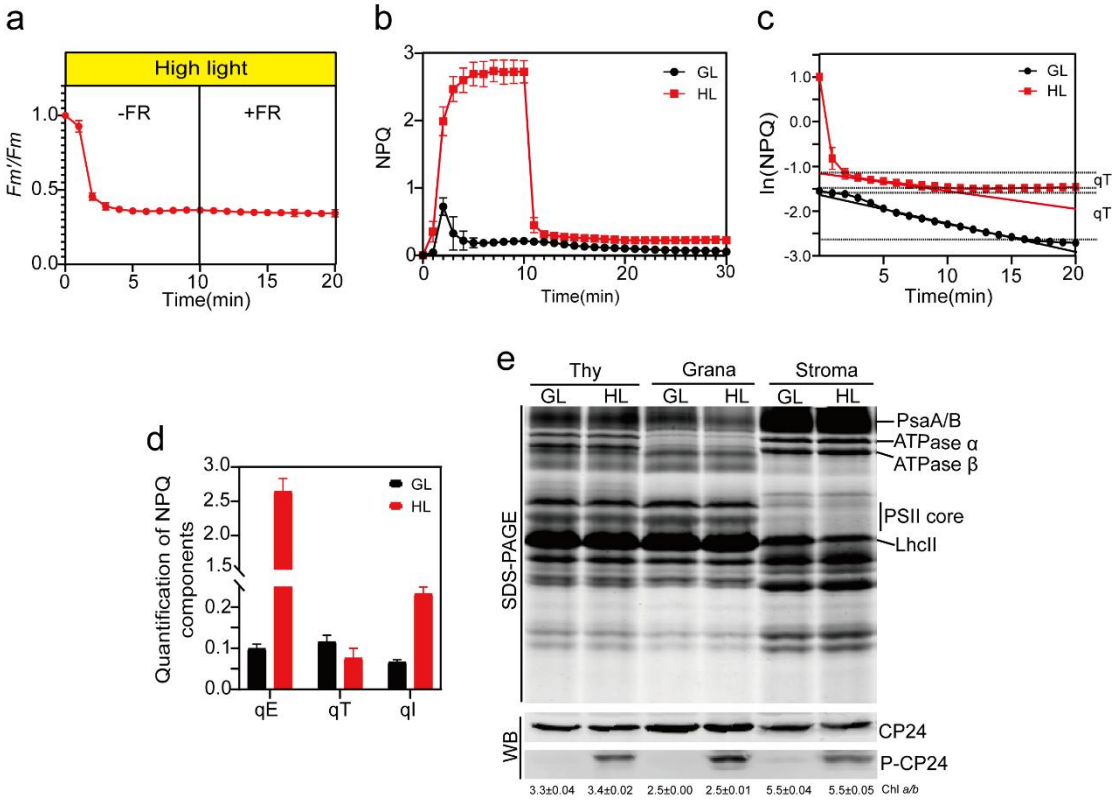

Figure 6: Assays of state transition and resolution of NPQ components

a Demonstration of state transition by controlling the presence or absence of FR under a HL background. **b** NPQ kinetics of *B. incana* was measured with actinic light at 100 µmol photons m^{-2} s^{-1} (GL) and 1000 µmol photons m^{-2} s^{-1} (HL), respectively. **c** Semi-logarithmic plots of NPQ. The data from the dark relaxation for 20 min in (**b**) were used to generate Semi-logarithmic plots. These plots illustrate the contribution of qT (state transitions) to NPQ. **d** Quantification of the three components of NPQ (qE, qT and qI). The quantification was based on the semi-logarithmic plots of NPQ in (**c**). **e** Localization of P-CP24 and CP24 in thylakoid membranes fractions. Thylakoid membrane fractions (grana and stroma-enriched) were isolated from plants grown under GL (100 µmol photons m^{-2} s^{-1}) or exposed to HL (1000 µmol photons m^{-2} s^{-1}) for 2 hours. These fractions were subsequently separated by SDS-PAGE. The localization of P-CP24 and total CP24 was determined by immunoblotting using anti-P-Thr and anti-CP24 antibodies, respectively. The chlorophyll *a/b* ratio (Chl *a/b*) for each sample was indicated below the corresponding lane. Thylakoid membrane samples were loaded with 5 µg Chl, while other fractions were loaded with 5 µg Chl. All data points, represented by symbols, and error bars denote the mean ± SD derived from a minimum of three independent biological replicates.

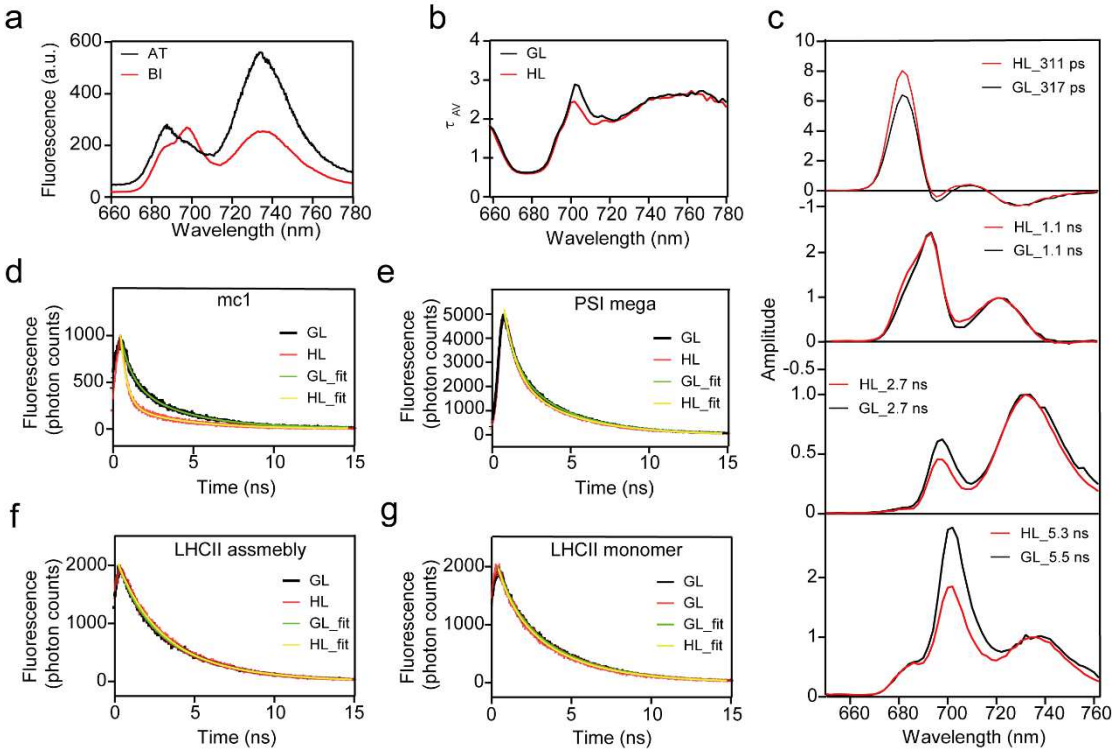

Figure 7: CP24 phosphorylation promotes the transfer of energy captured by CP47 to PSI

a 77 K fluorescence emission spectra of thylakoid membrane isolated from *B. incana* (red line) and *A. thaliana* (black line). Samples were excited at 436 nm. **b** Fluorescence average lifetime (τ_{AV}) of thylakoid membranes isolated from *B. incana* grown under growth light (GL) and exposed to high light (HL). **c** Time-resolved fluorescence decay-associated spectrum (DAS) analysis of thylakoid membranes isolated from *B. incana* grown under GL and HL conditions.. The DAS were normalized at PSI maximum fluorescence of the corresponding lifetime components. The sample was excited at 480 nm at 2 µg Chl mL^{-1}. (**d – g**) Time-correlated single-photon counting of fluorescence recorded at 695 nm for different thylakoid membrane complexes separated by lpCN-PAGE (Supplementary Fig. 8): **d** mc1, **e** PSI-megacomplexes, **f** LHCII assembly, **g** LHCII monomer.

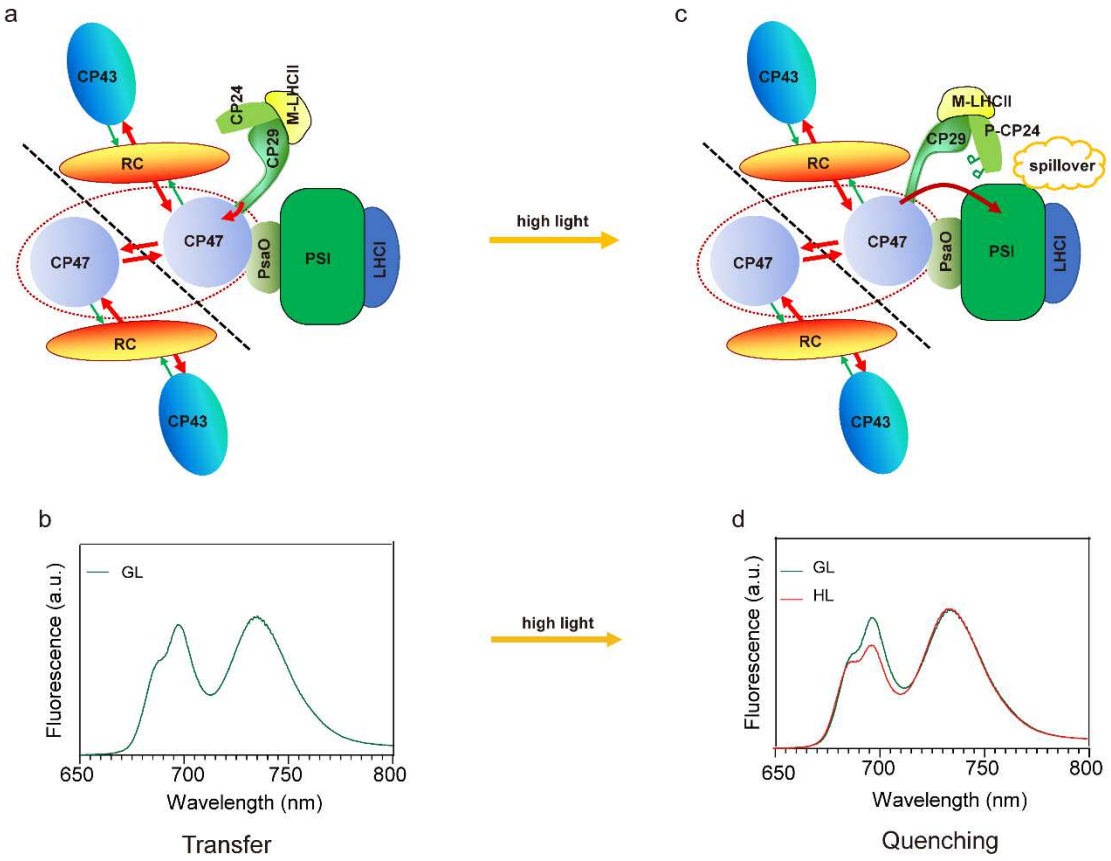

Figure 8: A model of CP24 phosphorylation enhancing qE via spillover regulation

a Energy pool formation by low-Energy CP47 domains in PSII supercomplexes. Under GL, two low-energy CP47 domains at the center of dimeric PSII supercomplexes form an energy pool (red ellipse). Energy preferentially transfers to CP47 (indicated by red arrows for energy upconversion and green arrows for energy downconversion in *B. incana*), establishing a photoprotective mechanism even under moderate light intensity. This process limits energy transfer to high-energy PSII core units, which remain susceptible to photodamage despite low-light conditions. **b** Energy accumulation in CP47 in GL in *B. incana*. The accumulation of energy in CP47 is evidenced by a pronounced fluorescence emission peak at 695 nm in fluorescence emission spectrum. **c** CP24 phosphorylation-induced spillover under HL. Transition from GL to HL conditions triggers massive phosphorylation of the minor PSII antenna protein CP24, inducing conformational changes that facilitate energy transfer from CP47 to PSI. This promotes spillover, a process redirecting excess energy away from PSII. **d** P-CP24 promotes spillover for photoprotection via PSI-mediated energy dissipation. CP24 phosphorylation enhances spillover efficiency, accelerating CP47-to-PSI energy transfer. Energy quenching in PSI reduces the fluorescence emission peak at 695 nm, alleviating excitation pressure on PSII at the molecular level.

Supplementary Files

This is a list of supplementary files associated with this preprint. Click to download.

- supplementaryinformation.pdf
- SupplementaryTable1.xlsx
- SupplementaryTable2.xlsx